JGR Atmospheres

RESEARCH ARTICLE
10.1029/2018JD029728

Structure, Variability, and Mean-Flow Interactions of the January 2015 Quasi-2-Day Wave at Middle and High Southern Latitudes

David C. Fritts[1], Hiroyuki Iimura[1], Diego Janches[2], Ruth S. Lieberman[2], Dennis M. Riggin[1], Nicholas J. Mitchell[3], Robert A. Vincent[4], Iain M. Reid[4,5], Damian J. Murphy[6], Masaki Tsutsumi[7], Andrew J. Kavanagh[8], Paulo P. Batista[9], and Wayne K. Hocking[10]

[1]GATS, Boulder, CO, USA, [2]NASA Goddard Space Flight Center, Greenbelt, MD, USA, [3]Department of Electronic and Electrical Engineering, University of Bath, Bath, UK, [4]School of Physical Sciences, University of Adelaide, Adelaide, South Australia, Australia, [5]Atrad Pty Ltd, Thebarton, South Australia, Australia, [6]Department of the Environment and Energy, Kingston, Tasmania, Australia, [7]National Institute of Polar Research and The Graduate University of Advanced Studies, Tokyo, Japan, [8]British Antarctic Survey, Cambridge, UK, [9]Instituto Nacional de Pesquisas Espaciais, São Paulo, Brazil, [10]Department of Physics, University of Western Ontario, London, Ontario, Canada

Abstract The structure, variability, and mean-flow interactions of the quasi-2-day wave (Q2DW) in the mesosphere and lower thermosphere during January 2015 were studied employing meteor and medium-frequency radar winds at eight sites from 23°S to 76°S and Microwave Limb Sounder (MLS) temperature and geopotential height measurements from 30°S to 80°S. The event had a duration of ~20–25 days, dominant periods of ~44–52 hr, temperature amplitudes as large as ~16 K, and zonal and meridional wind amplitudes as high as ~40 and 80 m/s, respectively, at middle and lower latitudes. MLS measurements enabled definition of balance winds that agreed well with radar wind amplitudes and phases at middle latitudes where amplitudes were large and quantification of the various Q2DW modes contributing to the full wave field. The Q2DW event was composed primarily of the westward zonal wavenumber 3 (W3) mode but also had measurable amplitudes in other westward modes W1, W2, and W4; eastward modes E1 and E2; and stationary mode S0. Of the secondary modes, W1, W2, and E2 had the larger amplitudes. Inferred MLS balance winds enabled estimates of the Eliassen-Palm fluxes for each mode, and cumulative zonal accelerations that were found to be in reasonable agreement with radar estimates from ~35°S to 70°S at the lower altitudes at which radar winds were available.

Key Points:
- The January 2015 quasi-2-day wave in the Southern Hemisphere was characterized by radar wind measurements and MLS limb observations
- The dominant mode was westward zonal wavenumber 3 (W3), but W1, W2, W4, E1, E2, and S0 also had measurable amplitudes and effects
- Balance winds derived from the MLS geopotential height and temperature measurements agree reasonably with meteor radar measurements

Supporting Information:
- Supporting Information S1
- Movie S1
- Movie S2
- Movie S3

Correspondence to:
D. C. Fritts,
dave@gats-inc.com

Citation:
Fritts, D. C., Iimura, H., Janches, D., Lieberman, R. S., Riggin, D. M., Mitchell, N. J., et al. (2019). Structure, variability, and mean-flow interactions of the January 2015 quasi-2-day wave at middle and high southern latitudes. *Journal of Geophysical Research: Atmospheres*, *124*, 5981–6008. https://doi.org/10.1029/2018JD029728

Received 25 SEP 2018
Accepted 25 MAR 2019
Accepted article online 2 MAY 2019
Published online 18 JUN 2019

Author Contributions:
Conceptualization: David C. Fritts, Dennis M. Riggin
Formal analysis: Hiroyuki Iimura
Funding acquisition: David C. Fritts, Diego Janches, Dennis M. Riggin, Iain M. Reid, Damian J. Murphy
(continued)

1. Introduction

The quasi-2-day wave (Q2DW) is a global planetary-scale phenomenon and episodically one of the most prominent features in atmospheric dynamics in the mesosphere and lower thermosphere (MLT). It has been observed in many fields throughout the atmosphere over the ~4 decades since its discovery (Glass et al., 1975; Kashcheyev & Oleynikov, 1999; Muller & Kingsley, 1974; Muller & Nelson, 1978). An early general circulation model study by Hunt (1981) reproduced the Q2DW in the wind and temperature fields and inferred that the Q2DW is a westward propagating, zonal wavenumber 3 (W3) mode having a very small phase variation with altitude, in agreement with the observations by Rogers and Prata (1981).

Salby (1981a) proposed that the Q2DW was a manifestation of the mixed Rossby-gravity (3,0) normal mode of a windless, isothermal atmosphere with a period of ~2.25 days. Salby (1981b, 1981c) also investigated responses of various Rossby normal mode wind and temperature fields to nonuniform mean winds and temperatures. He concluded that Q2DW frequencies were largely influenced by the mean wind and that amplitude growth with altitude was enhanced in regions of increased refractive index by weak zonal winds and decreasing equatorward temperatures. Hagan et al. (1993) used a linear spectral model for January mean conditions and found evidence of the Q2DW in the mesosphere as the westward propagating mixed Rossby-gravity (3,0) normal mode, as initially proposed by Hunt (1981) and Salby (1981a) and observed by Rogers and Prata (1981). Hagan et al. (1993) also found that a combination of weak eastward winds in the winter hemisphere and westward winds in the summer hemisphere increased mode amplitudes at low and middle latitudes in the summer hemisphere.

Investigation: David C. Fritts, Hiroyuki Iimura, Nicholas J. Mitchell
Methodology: David C. Fritts, Hiroyuki Iimura, Ruth S. Lieberman
Resources: Diego Janches, Nicholas J. Mitchell, Robert A. Vincent, Iain M. Reid, Damian J. Murphy, Masaki Tsutsumi, Andrew J. Kavanagh, Paulo P. Batista, Wayne K. Hocking
Software: Ruth S. Lieberman, Wayne K. Hocking
Writing - original draft: David C. Fritts
Writing – review & editing: David C. Fritts

Plumb (1983) and Pfister (1985) proposed that the Q2DW could be forced by baroclinic instability of the zonal jet in the summer mesosphere. Additional assessments using various global models confirmed that the Q2DW is primarily a Rossby-gravity (3,0) mode arising from baroclinic and/or barotropic instabilities (McCormack et al., 2009; Norton & Thuburn, 1996; Salby & Callagham, 2001, 2003; Schröder & Schmitz, 2004; Yue et al., 2012). Studies by Palo et al. (1999) and Froehlich et al. (2003) also described the Q2DW structure and suggested that it could be excited in the lower atmosphere and propagate into the MLT.

Additional studies employing ground-based and satellite measurements examined Q2DW occurrence statistics, structure, periods, and interactions with other waves. Multiple studies addressed variations with season and latitude and confirmed the major contributions by W3 (Azeem et al., 2001; Baumgaertner et al., 2008; Clark et al., 1994; Ern et al., 2013; Garcia et al., 2005; Huang et al., 2013; Lilienthal & Jacobi, 2015; Limpasuvan & Wu, 2003; Malinga & Ruohoniemi, 2007; Nozawa et al., 2003; Offermann et al., 2011; Rogers & Prata, 1981). Others revealed a tendency for larger amplitudes and more temporally isolated responses in the Southern Hemisphere (SH; Gu, Li, Dou, Wu, et al., 2013; Huang et al., 2013; Limpasuvan et al., 2005; Wu et al., 1993, 1996), typically larger meridional than zonal amplitudes (Fritts & Isler, 1994; Gu, Li, Dou, Wu, et al., 2013; Ward et al., 1996), and very large vertical wavelengths, $\lambda_z > 100$ km, in the MLT (Tsuda et al., 1988). Several studies estimated the Eliassen-Palm (EP) fluxes that were able to be computed with available data (France et al., 2018; Fritts et al., 1999; Lieberman, 1999).

Westward modes with zonal wavenumbers 2 and 4 (W2 and W4) and eastward modes E1 and E2, with the graver modes having longer periods, were inferred by multiple authors (Ern et al., 2013; Gu, Li, Dou, Wu, et al., 2013; Limpasuvan & Wu, 2009; Malinga & Ruohoniemi, 2007; Meek et al., 1996; Merzlyakov et al., 2004; Pancheva et al., 2004; Riggin et al., 2004; Thayaparan et al., 1997; Tunbridge et al., 2011). Others suggested that E2 can comprise the major response in the winter MLT (Pancheva et al., 2018; Sandford et al., 2008; Xian et al., 2013) and a potential for Q2DW penetration to much higher altitudes (Moudden & Forbes, 2014; Ward et al., 1996).

Additional studies provided evidence of interactions of the Q2DW with tides and gravity waves (GWs), and a potential for these interactions to have influences at higher altitudes and latitudes (Forbes & Moudden, 2012; Gu, Li, Dou, Wang, et al., 2013; Hecht et al., 2010; Jacobi et al., 2006; Lieberman et al., 2017; McCormack et al., 2010; Nguyen et al., 2016; Palo et al., 2007; Pancheva, 2006). More recently, France et al. (2018) showed that the 2014 Q2DW Northern Hemisphere (NH) event was likely responsible for an anomalous decline in NH polar mesospheric clouds (PMCs) during that summer season. Importantly, however, there have been no studies to date that attempted to provide broad hemispheric definition of a significant Q2DW event using both satellite and extensive ground-based measurements and an intercomparison of these observations to assess the ability to quantify the Q2DW fields, the Q2DW modes contributing most to its structure and variability, and its interactions with the large-scale flow.

In this paper, we use both radar wind measurements and Aura Microwave Limb Sounder (MLS) temperature and geopotential height measurements and inferred horizontal winds to quantify the structure and evolution of the SH Q2DW event occurring in January 2015. Computed quantities include the Q2DW modal composition and amplitudes, its spatial and temporal variations, and its EP fluxes and divergence. Our data acquisition and analysis procedures and the balance equation enabling computation of winds and EP fluxes are described in section 2. Section 3 describes our analyses of the radar and MLS data, respectively. We discuss our results relative to previous Q2DW studies in section 4. Our conclusions are provided in section 5.

2. Data Acquisition and Analysis

2.1. Meteor and Medium-Frequency Radars

One component of our Q2DW analysis was performed using meteor radar winds at Cachoeira Paulista (23°S, 45°W; hereafter CP), Adelaide (35°S, 138°E), Kingston (43°S, 144°E), Tierra del Fuego (54°S, 68°W; hereafter TdF), and Rothera (68°S, 68°W), and medium-frequency (MF) radar winds at Rothera, Davis (68°S, 78°E), Syowa (69°S, 40°E), and Halley (76°S, 25°W); see Figure 1. To assess the consistency between meteor and MF radars, we compare Q2DW amplitude and phase assessments using the two radars at Rothera. Our radar data analysis included the following steps:

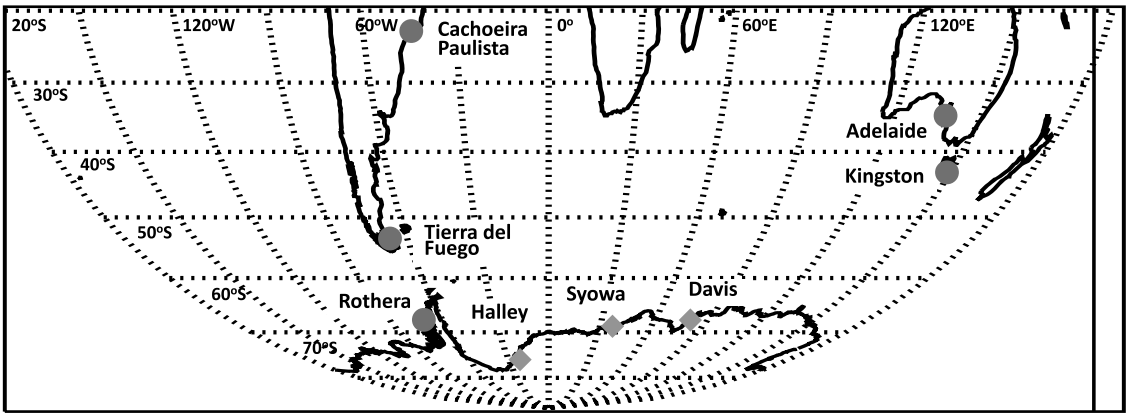

Figure 1. Locations of meteor and medium-frequency radars employed for this study. Circles denote meteor radars, diamonds denote medium-frequency radars, and Rothera has both types.

1. Hourly horizontal wind estimates were performed where at least five radial wind estimates were available in 2-km altitude bins at Adelaide, Kingston, Rothera (MF), Davis, Syowa, and Halley and in 3-km bins at CP, TdF, and Rothera (meteor);
2. Missing hourly winds at each altitude were interpolated with 3 degrees of freedom for intervals less than 12 hr; intervals between 12 and 48 hr were fitted with a linear trend and components having periods of 8, 12, 24, and 48 hr consistent with adjacent radar data in order to enable S-transform and band-pass analyses using continuous data;
3. A band-pass filter from 42 to 54 hrs centered on the expected W3 period of 48 hr, and including the periods of other prominent Q2DW modes, was applied to the resulting hourly-mean radar winds from December 2014 to February 2015;
4. As in previous planetary wave (PW) studies using MLT radar winds (Fritts et al., 2012; Iimura et al., 2015), the S-transform (Stockwell et al., 1996) was used to assess the event periods and durations using a Gaussian 10-day full-width/half-maximum window; however, intervals of missing data longer than 12 hr were left blank in the relevant figures;
5. the S-transforms were used to infer the optimal Q2DW period and amplitude fit at each altitude for comparisons with MLS inferred winds at the radar sites, and
6. local Q2DW amplitudes and phases at each altitude were estimated by least squares fits to sinusoids with periods having the maximum amplitudes in the S-transform spectra.

S-transform Q2DW amplitudes were compared with those from the band-passed hourly time series and seen to exhibit maximum differences of ~10%. Radar amplitudes were also averaged using a 10-day sliding window for comparisons with those inferred from MLS measurements.

2.2. Aura MLS

NASA's Earth Observing System Aura satellite was launched on 15 July 2004 into a Sun-synchronous orbit at an altitude of 705 km. Aura performs nearly 15 orbits per day, crossing the equator at 13:30 LT (01:30 LT) on ascending (descending) northward (southward) passes. MLS began providing data on 13 August 2004. It measures atmospheric temperature and chemical constituents at pressures from 1,000 to 10^{-5} hPa (Waters et al., 2006) from 82°N and 82°S on every orbit. Geopotential height is computed from integration of the hydrostatic equation (Schwartz et al., 2008).

Aura/MLS geopotential height data were collected in bins of 24° in longitude, 5° in latitude from 30°S to 80°S, and 12-hr universal time (UT) at eight pressure levels from 0.05 to 2×10^{-4} hPa. The levels employed for our studies here correspond to altitudes of ~70, 76, 81, 86, 91, 97, 103, and 107 km. These data enabled running 10-day least squares fits to sinusoids with zonal wavenumbers, $s = -2$ to $+3$, for a 1-day period (except the migrating diurnal tide, DW1), $s = -4$ to $+2$ for a 2-day period, $s = -2$ to $+1$ for a 4-day period, and $s = -1$ for 5- and 10-day periods, where negative s indicates westward propagation. The Sun-synchronous Aura orbit implies that the migrating diurnal and semidiurnal tides (DW1 and SW2) project to the daily zonal mean and therefore do not alias to the Q2DW or other large-scale motion fields.

Temporal variability in the tidal and larger-scale PW fields may nevertheless alias to apparent Q2DW modes, where their amplitudes are significant. The implications of this possibility for our study are discussed below.

Given the largely absent migrating tide aliasing, we expected the 2-day period fits to yield good amplitude and phase estimates for the various Q2DW modes. Furthermore, aliasing tests showed that Q2DW W3 amplitudes changed by only ~10% by including the $s = \pm 3$ modes for other periods. Thus, we excluded E3 for the Q2DW and $s = \pm 3$ for the 4-, 5-, and 10-day periods from the fittings, under the assumption that these modes had negligible impacts on the Q2DW fits.

Amplitudes and phases of Q2DW modes in the zonal and meridional winds were estimated from Q2DW geopotential height amplitudes and phases obtained from the above fittings for each Q2DW mode using the zonal and meridional momentum equations (Hitchman et al., 1987)

$$\partial u'/\partial t + U_0(\partial u'/\partial \lambda)/(a\ \cos\phi) - f_1 v' = -(\partial \Phi'/\partial \lambda)/(a\ \cos\phi) \tag{1}$$

$$\partial v'/\partial t + U_0(\partial v'/\partial \lambda)/(a\ \cos\phi) + f_2 u' = -(\partial \Phi'/\partial \phi)/a \tag{2}$$

To enable these estimates, zonal mean zonal winds were estimated from zonal mean geopotential heights, assuming gradient wind balance (Hitchman & Leovy, 1987; Hitchman et al., 1987). A scale analysis of the meridional momentum equation (Nguyen, 2016) yields the relation

$$U_0[f + U_0(\tan\phi/a)] = -\partial \Phi'/\partial y \tag{3}$$

Assuming approximate hydrostatic equilibrium (Nguyen, 2016) then yields the following

$$U_0 = -(1/f)(\partial \Phi'/\partial y)[1-(1/f)(\partial \Phi'/\partial y)/(2\Omega\ a\ \cos\phi)]^{-1} \tag{4}$$

Here and below, U_0 is zonal mean zonal wind; (u',v',w'), Φ', and T' are perturbation velocities, geopotential height, and temperature; ϕ and λ are latitude and longitude; a is Earth's radius, $\Omega = 2\pi$ day^{-1}; N and ω_i are buoyancy and intrinsic frequencies; and f_1 and f_2 are defined as

$$f_1 = 2\Omega\ \sin\phi - [\partial(U_0\ \cos\phi)/\partial\phi]/(a\ \cos\phi) \tag{5}$$

$$f_2 = 2\Omega\ \sin\phi + 2U_0\ \tan\phi/a \tag{6}$$

The tendencies in equations (1) and (2) were assessed using 1-hr differences of the total fields.

Nguyen (2016) validated Q2DW winds computed via equations (1)–(4) using pseudo-data from the NCAR Whole Atmosphere Community Climate Model (WACCM) at 86 km. Agreement between WACCM and Q2DW winds derived from equations (1)–(4) was excellent poleward of 30°. Following Hitchman et al. (1987), Nguyen introduced a frictional term to remove singularities near latitudes where the Q2DW frequency approaches the zonal mean absolute vorticity. In practice, this adjustment was required in the vicinity of 20°N and 20°S. Sharp latitudinal gradients in the wind amplitude were observed at low latitudes, implying that singular solutions do affect the wind estimates. However, the radar sites discussed in this paper are situated well poleward of the Q2DW singular latitudes.

Finally, it should be noted that GW drag on planetary-scale MLT winds will affect the momentum balance described in equations (1)–(4); see Smith (1996), Meyer (1999), and Lieberman et al. (2013). Given the good agreement with WACCM noted by Nguyen (2016), however, we do not include these effects in equations (1)–(4).

The inferred Q2DW amplitudes and phases enabled computation of the EP fluxes (Andrews et al., 1987) given by

$$F^{\phi} = \rho_0 a\ cos\ \phi[(\partial U_0/dz)<v'\theta'>/(\partial \theta_0/dz) - <u'v'>] \tag{7}$$

$$F^{z} = \rho_0 a\ cos\ \phi\left\{\left[f - (a\ cos\ \phi)^{-1}\ \partial(U_0\ cos\ \phi)/d\phi\right]<v'\theta'>/(\partial \theta_0/dz) - <u'w'>\right\} \tag{8}$$

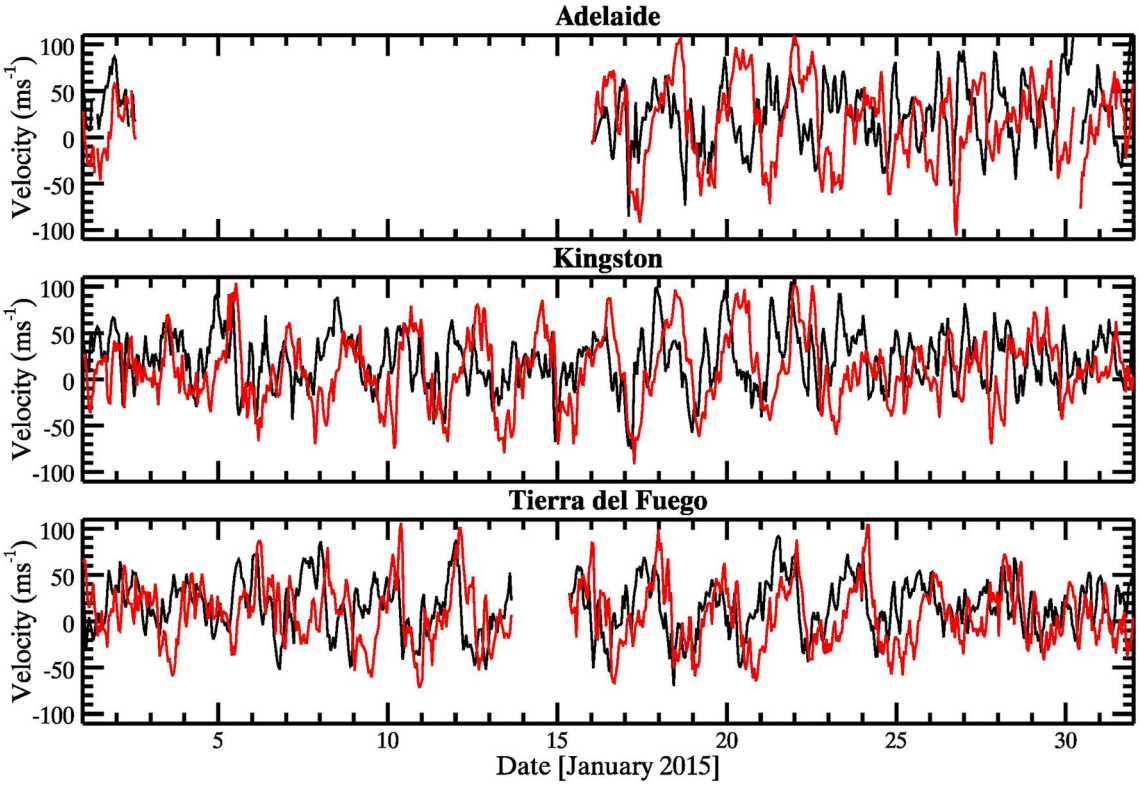

Figure 2. (black and red) Meteor radar zonal and meridional hourly winds at Adelaide, Kingston, and TdF at 90 km throughout January 2015. Note the dominant Q2DW at each site.

which can be assessed with MLS measurements and inferred winds (validated by meteor and MF radars), where ρ_0, θ_0, θ', and z are mean density, mean and perturbation potential temperature, and altitude. The Q2DW had $T'/T < 0.1$ in the MLT; hence, $w' \sim (g/N^2)(T'/T)\omega_i \sim 0.02$ m/s (with gravitational constant g), yielding $<u'w'> \sim 0.4$ m/s in equation (8). GWs also contribute a mean $<u'w'> \sim$ 5–10 m/s/day based on measurements, modeling, and theory (Fritts & Alexander, 2003; Richter et al., 2010; VanZandt & Fritts, 1989), and this will be seen in section 3.5 to cause much larger EP flux divergences than the dominant Q2DW contributions during this event, as expected given the known mean GW forcing of the cold summer mesopause at polar latitudes.

3. Results

3.1. Radar Q2DW Winds

Hourly zonal and meridional winds computed as described above are shown in Figure 2 for the radars at Adelaide, Kingston, and TdF spanning the Q2DW event at southern latitudes in January 2015. These plots reveal that the dominant contributor to zonal and meridional winds from ~5 to 25 January at each site was the Q2DW. Also seen are sporadic bursts of apparent diurnal and semidiurnal tide responses and inertia GWs at higher frequencies, but the amplitudes of these other motions are in almost all cases smaller than those of the Q2DW. There is also no evidence of longer-periods PWs during this interval nor in an S-transform including these PW periods.

Figure 3 compares 2-day and 10-day mean Q2DW amplitudes and phases obtained with the meteor radars at Kingston and TdF, and with the meteor and MF radars at Rothera, throughout the January 2015 event. The comparisons employ the radar winds at the altitudes nearest the MLS altitude of 91 km, as radar and MLS winds will be intercompared below. 10-day mean radar winds are shown because a 10-day mean is required to enable full determination of the Q2DW using asynoptic sampling by MLS. Fits at Rothera are provided for both the meteor and MF radars in order to compare the measurements between the two radar types.

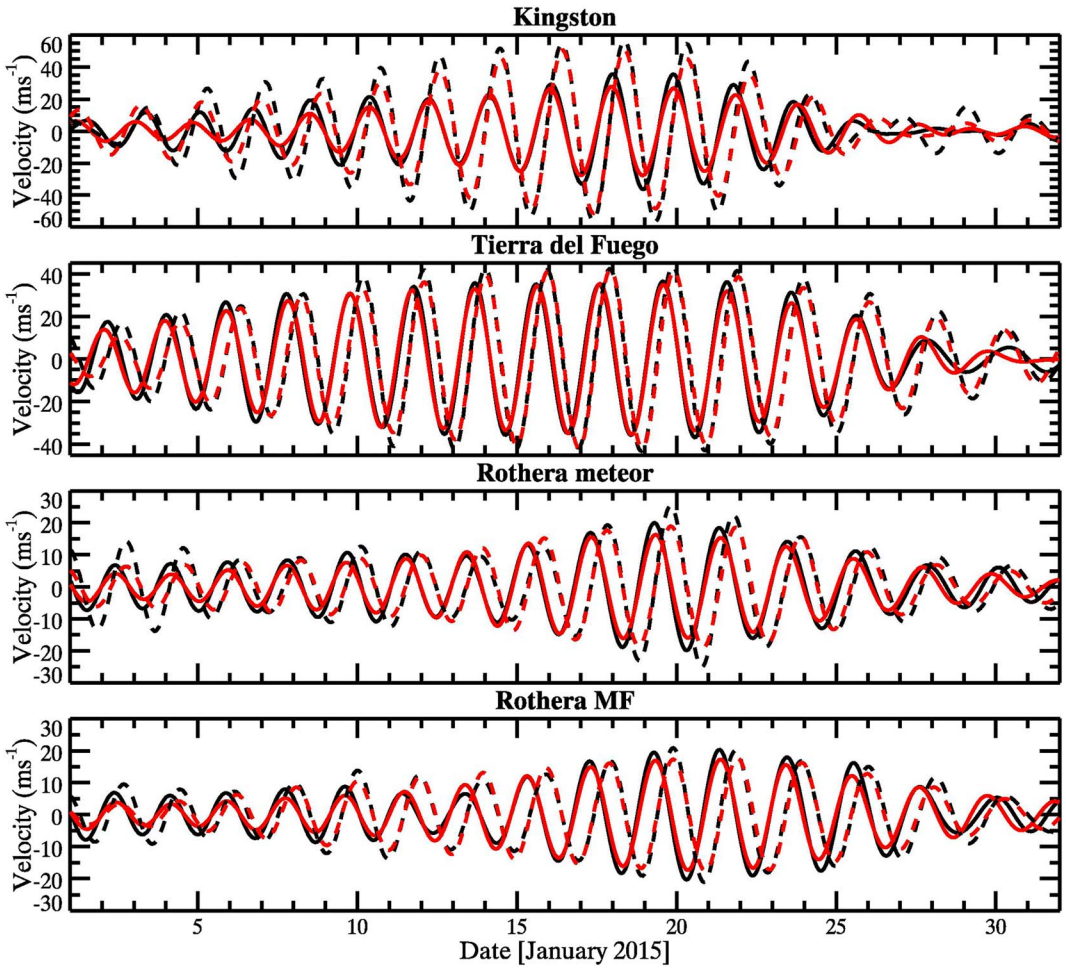

Figure 3. Meteor radar zonal and meridional Q2DW winds (solid and dashed) at Kingston, TdF, and Rothera at 90 km using 2-day and 10-day (full-width/half-maximum) sliding Gaussian fits (including both radars at Rothera). Black (red) lines denote 2-day (10-day) fits.

The two averaging intervals are seen to yield close agreement in amplitude and phase where amplitude growth and/or decay are sustained over multiple Q2DW cycles (e.g., growth and decay over TdF and the growth phase over Rothera seen by the meteor radar). Differences arise, as expected, near transient maxima (e.g., the narrow maxima at Kingston and slightly later maxima at Rothera).

Comparing the Q2DW responses obtained with the meteor and MF radars at Rothera (note the different scales in the lower two panels), we see similar phases and amplitudes prior to 10 January and after 22 January but smaller amplitudes with the MF radar between these dates, especially in the meridional component. A possible cause for these differences is the asymmetric receiver system for the MF radar, which is somewhat elongated in the N-S direction. We believe the meteor radar measurements to be more reliable in cases where there are clear differences.

Q2DW responses at these sites exhibit both similarities and differences. The largest amplitudes, and the largest differences between zonal and meridional components, occurred at Kingston, where 2-day means were ~35 and 55 m/s at the event peak. By comparison, peak Q2DW zonal and meridional winds at TdF were ~35 and 43 m/s at the same time.

The largest Q2DW winds on 1 January near the event onset occurred at TdF and approached 20 m/s in both components. Meridional amplitudes at Kingston overtook those at TdF on ~10 January, but zonal amplitudes at Kingston only became comparable to those at TdF on ~17 January, due to the larger component wind differences throughout the event at Kingston. Following the peak amplitudes on ~17 January, the Kingston wind components also decayed more rapidly. As at TdF, zonal Q2DW winds at Rothera were

comparable to or smaller than meridional winds. Additionally, peak zonal Q2DW winds at Rothera were roughly half (or less) than those at Kingston and TdF. The evolutions of the Q2DW EP fluxes and zonal mean wind over this interval are described in section 4 below.

We employed the S-transform (Stockwell et al., 1996) to assess the dominant periods using measurements at 90 km. We also used a 42- to 54-hr band-pass filter to define Q2DW u' and v' amplitudes for each radar throughout the event from 84 to 93 km. The radars typically measure winds from ~80 to 100 km, but reduced meteor counts at the lowest and highest altitudes caused wind estimates to be more uncertain. Hence, we focus on the central, more confident wind estimates here. S-transform results are shown for all nine radars in Figure 4. Q2DW u' and v' amplitudes are shown in Figure 5, except for the Rothera MF radar, where the two radars yielded very similar results, and for Halley, due to absence of data during the strongest response.

Referring to Figure 4, we see that S-transform periods were variable at all sites. Those at Kingston increased from ~43 to 48 hr from ~8 to 17 January and decreased thereafter. Those at TdF generally increased from ~45 to 52 hr in both components from ~5 to 21 January. Available data at Adelaide were consistent with meridional observations at Kingston, where amplitudes were comparable, but inferred zonal periods were shorter where the zonal amplitudes were much smaller. Dominant periods were somewhat longer at CP than at higher latitudes, but this is not surprising, given that the CP response lacked coherence between u' and v' and appeared to be largely uncoupled to those at higher latitudes. Inferred periods at Rothera and higher latitudes were largely consistent with those seen at Kingston and TdF. This suggests that common dominant Q2DW modes defined the best fit periods from ~35°S to 76°S throughout this event, despite temporal amplitude variations due to varying mode phase speeds and superpositions. They also suggest a dominance of the middle- and high-latitude responses at the earlier times by the graver zonal wavenumbers, $s = 0, \pm1$, and ±2. This will be explored more fully in the discussion of MLS results below.

Figure 5 reveals that Q2DW amplitudes generally increased with altitude or achieved their maxima in this altitude range. The exceptions were u' at Adelaide at early times and at Kingston, both of which were larger at lower altitudes. We also note the general agreement of the times of peak amplitudes from 35° to 69°S (roughly centered in January), despite their very different measurement longitudes in several cases. The exceptions to this were (1) the much earlier u' maxima at CP and Adelaide and (2) the later v' maximum at CP.

Figure 5 also reveals that u' maxima at CP and Adelaide of ~25 m/s in middle to late January were significantly weaker than at Kingston and TdF, though they were nearly coincident in time. In contrast, v' amplitudes at CP and Adelaide were later or larger, respectively, than at either Kingston or TdF, which were $u' \sim 55$ and 45 m/s. Q2DW zonal and meridional amplitudes at higher latitudes were more closely correlated in time but were smaller than the maxima at middle latitudes by 50% or more. The clear differences in Q2DW response intervals at CP and Adelaide relative to those at middle and high latitudes suggest that the early response at both sites, and potentially the major CP response in v', was not related to the primary SH event.

We now examine Q2DW phase variations and coherence among six sites at longitudes extending from Rothera and TdF eastward to Kingston (68°W to 144°E or 630° of W3). Figure 6 shows zonal and meridional (left and right columns) phase variations with longitude and altitude (top and bottom rows), respectively, following the method employed by Pancheva et al. (2004). Mean phases were determined using a band-pass filter of 46–50 hr from 15 to 25 January 2015. Best fit phase variations of ~650° in each component at 90 km in the upper panels reveal descending phase with increasing longitude and imply primarily westward propagation and close agreement with the 636° expected for a W3 phase structure over this range of longitudes.

Phase variations with altitude at these sites (Figure 6, lower panels) reveal large vertical wavelengths and confirm that u' leads v' by 10–12 hr at intermediate and higher altitudes, consistent with the upper panels. Phase progression is downward at Adelaide and Kingston and is more rapid downward at TdF but is less well defined or reversed at the three Antarctic sites. Specifically, all sites poleward of Kingston have one or both Q2DW wind components exhibiting near-vertical or apparent ascending phase in time at some altitudes. These include Rothera, Syowa, and Davis in u' and TdF, Rothera, and Davis in v'. Wind component phases from the Rothera MF radar are also shown and confirm those obtained with the Rothera meteor radar in u' but suggest stronger upward propagation than the Rothera meteor radar in v'. Finally, Adelaide suggests overall phase descent, except between 88 and 92 km in the zonal component. Collectively, this variability at multiple sites suggests a superposition of Q2DW modes throughout this event. Thus, we assess below

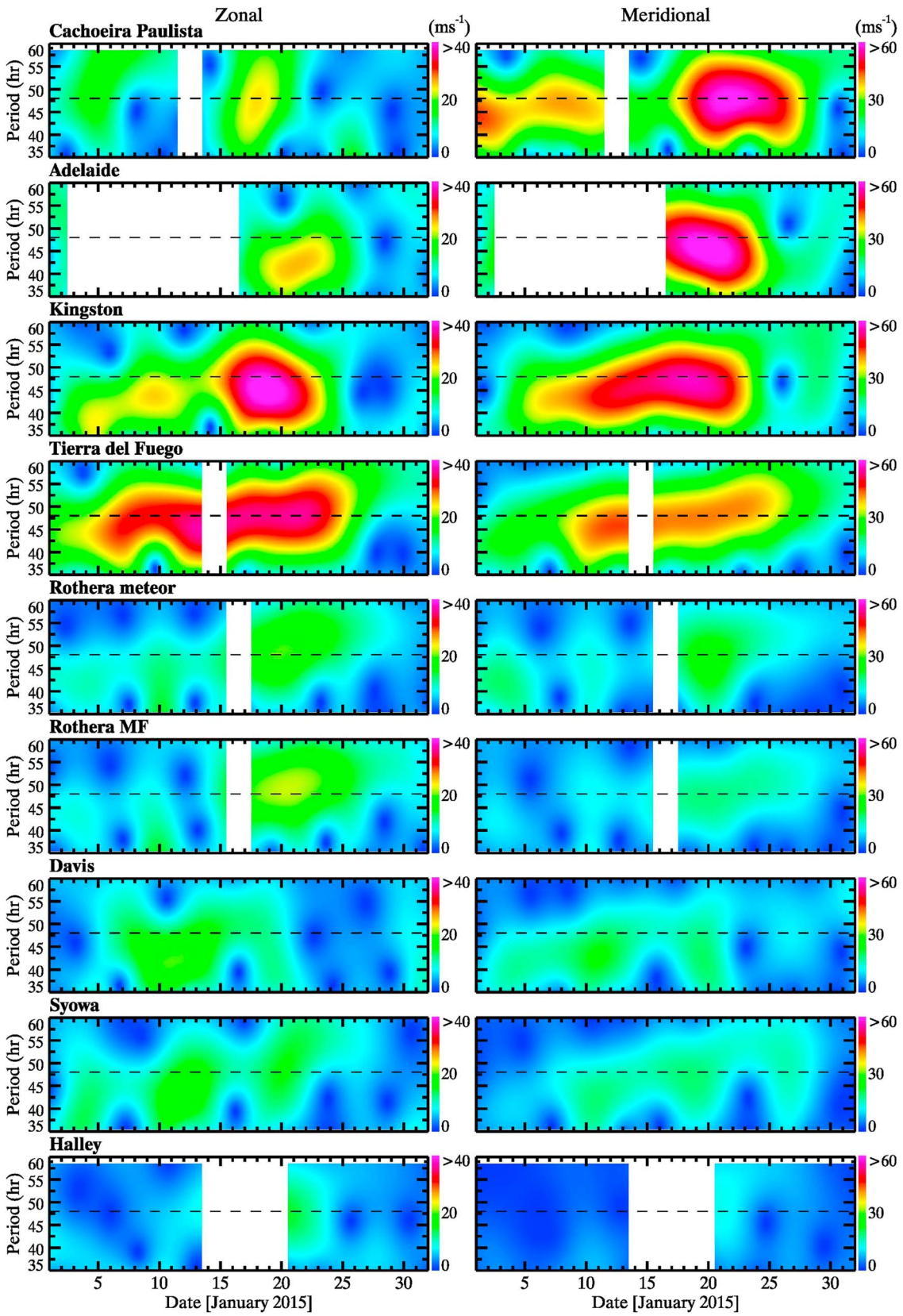

Figure 4. Dominant S-transform periods of zonal and meridional winds determined from radar measurements by nine radars at eight sites at 90 km in January 2015.

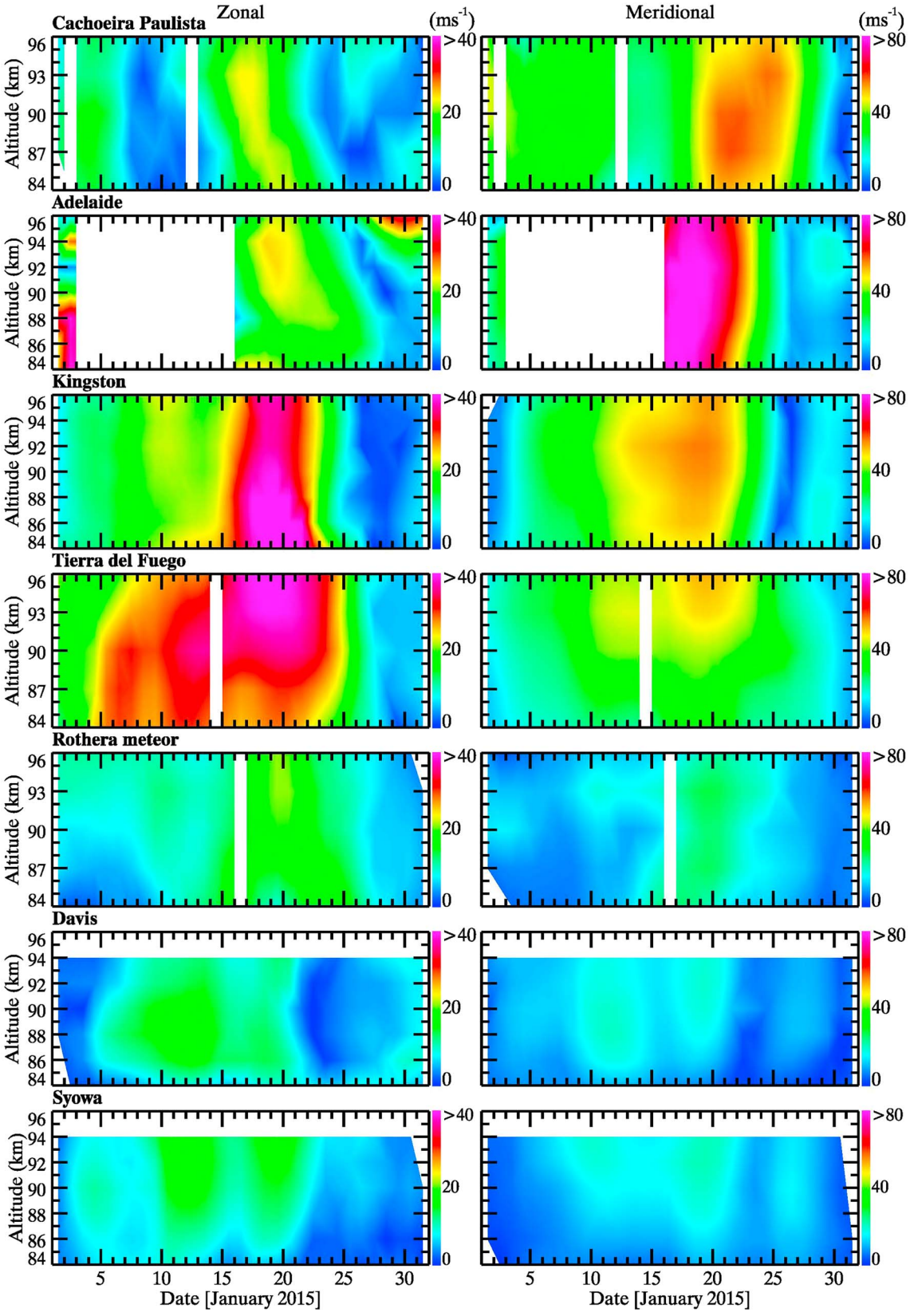

Figure 5. Q2DW zonal and meridional wind amplitudes (left and right columns) in January 2015 as a function of altitude from radar measurements at seven sites, top to bottom.

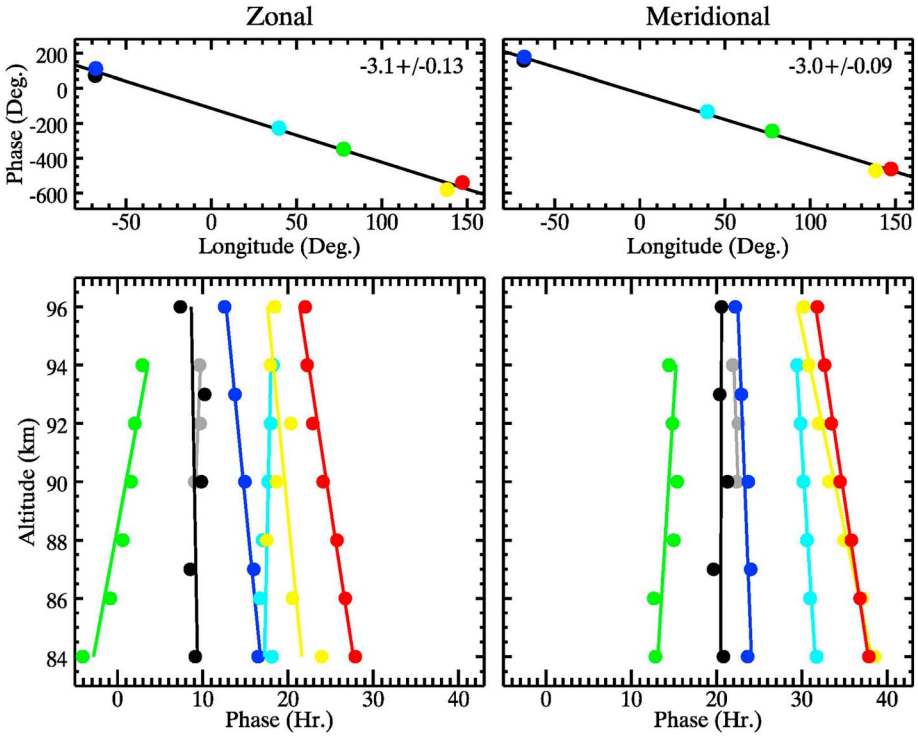

Figure 6. Mean Q2DW phases (top row) with longitude at 90 km and (bottom row) with altitude from 15 to 25 January 2015 for a band-pass filter from 44 to 52 hr with zonal (meridional) phases of maximum winds at left (right column), respectively. Color codes are Adelaide (yellow), Kingston (red), TdF (dark blue), Rothera meteor radar (black), Rothera MF radar (grey), Syowa (light blue), and Davis (green). Dots in lower panels show altitudes of radar winds, solid lines are least squares linear fits, and phases are shown in degrees of longitude (top row) and hours (bottom row).

the amplitudes and phase structures in space and time of the full and component Q2DW fields inferred from balance winds.

3.2. MLS Balance Winds and Temperatures

Balance winds from 30°S to 70°S inferred from MLS Φ and T from 20°S to 80°S at 91 km at 2-day intervals from 4 to 26 January at 00:30 UT are shown in Figure 7 (also see Movie S1 in the supporting information). These reveal a systematic growth and decay of the Q2DW spanning 11 cycles. The dominant Q2DW character throughout the evolution was W3, with largely counterclockwise winds in time at most locations and times. However, there were variations in the Q2DW structure that arose due to contributions by other modes throughout the evolution.

Q2DW balance winds and T' were largest at low to middle latitudes, for example, ~40–60 m/s at the latitude of TdF; T' maxima and minima exceeded 10 K at the latitude of Kingston, and v' and T' were largely anticorrelated. Q2DW wind vectors at Kingston, TdF, and Rothera (blue arrows in Figure 7) also reveal good agreement with MLS balance winds at these times (see further discussion below). Finally, a general, but slow, westward drift of the W3 pattern reveals a dominant period slightly shorter than 48 hr (see the counterclockwise rotations of the balance winds and T' from 8 to 22 January).

Departures of the full field from a W3 structure are seen at lower and higher latitudes. Those at lower latitudes suggesting advances of the phase structure at a zonal wavenumber other than W3 may not have been a part of this SH event (e.g., see the CP zonal and meridional wind maxima at earlier and later times, respectively) but were instead contributed by cross-equatorial influences from a NH response. At middle latitudes, W3 becomes prominent only slowly, by ~12 January, while other modes clearly contribute throughout; see especially the significant departures from a W3 response at large amplitudes beginning ~16 January. We also

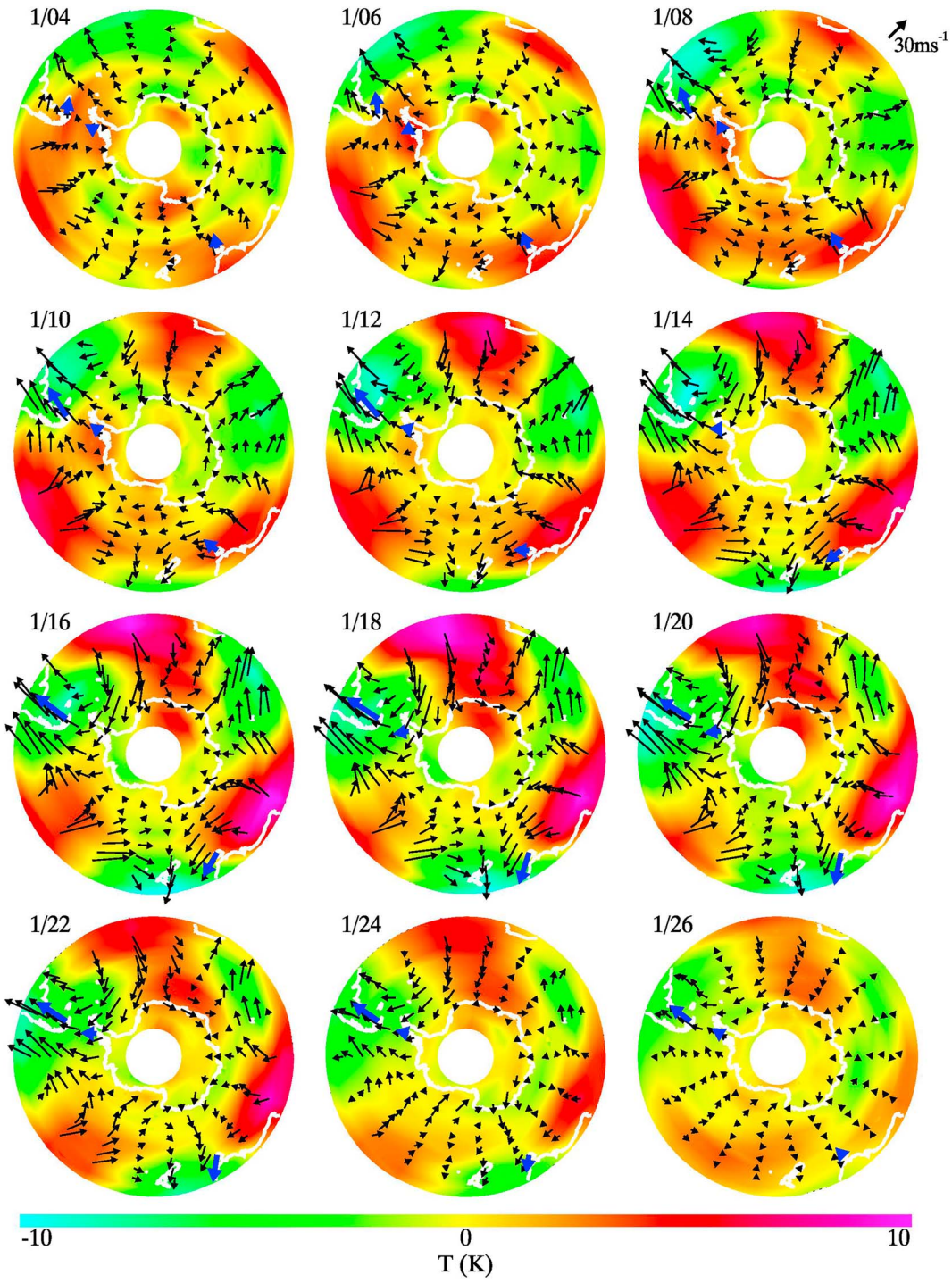

Figure 7. MLS balance winds and temperatures at 91 km at 00:30 UT from 4 to 26 January at intervals of 2 days. Blue arrows in each panel show the horizontal winds measured by the meteor radars at the same times at Kingston, TdF, and Rothera.

see that W3 is never large at high latitudes, where modes having zonal wavenumbers 1 and 2 appear to dominate (see the discussion of individual modes below).

We explore the agreement between MLS and radar winds in greater detail using measurements over Kingston, TdF, and Rothera (~43–68°S) spanning 6.5 Q2DW cycles from 12 to 25 January for which radar wind estimates were significant and nearly continuous. Because radar wind uncertainties depend on

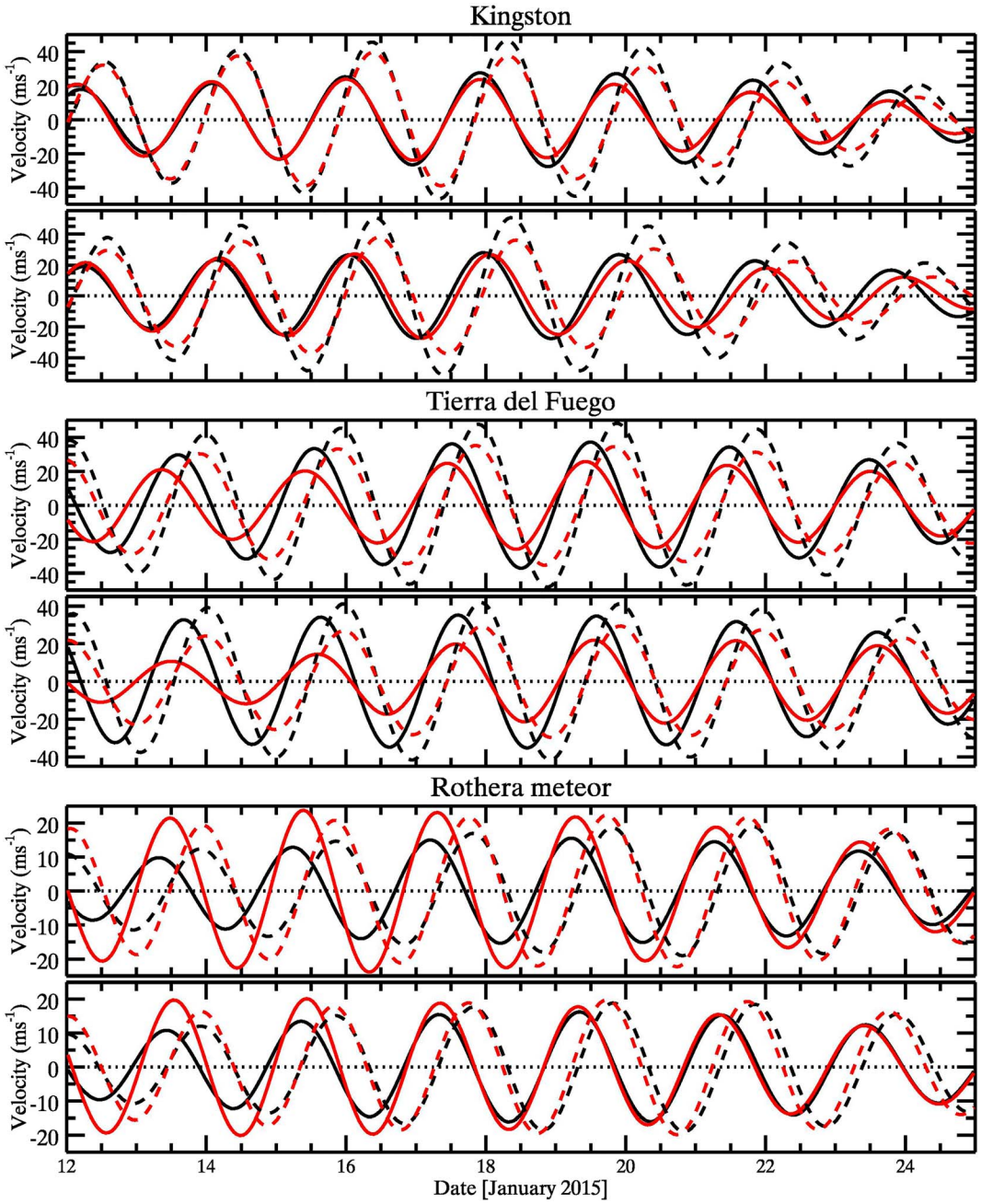

Figure 8. Time series of 10-day mean Q2DW amplitudes from 12 to 25 January 2015 at 97 and 91 km (top and bottom in each panel set) at Kingston, TdF, and Rothera (top to bottom). Solid and dashed lines indicate zonal and meridional winds, and black and red lines indicate meteor radar and MLS balance equation winds, respectively.

meteor counts, we performed these comparisons at ~91 and 97 km, for which radar measurements yielded confident wind estimates and MLS estimates were available. The results are shown in Figure 8. Comparisons of radar and MLS balance winds exhibit quite good agreement in Q2DW amplitude and phase at these altitudes at all three sites. In several cases, especially the first few cycles at Kingston, and the latter few cycles at Rothera, radar and MLS estimates of one or both wind components are virtually indistinguishable. Zonal winds typically led meridional winds by ~90°, indicating largely counterclockwise rotation of the Q2DW winds with time, and meridional winds were comparable to, or larger than, zonal winds. MLS winds at Kingston and TdF had comparable or smaller amplitudes than the

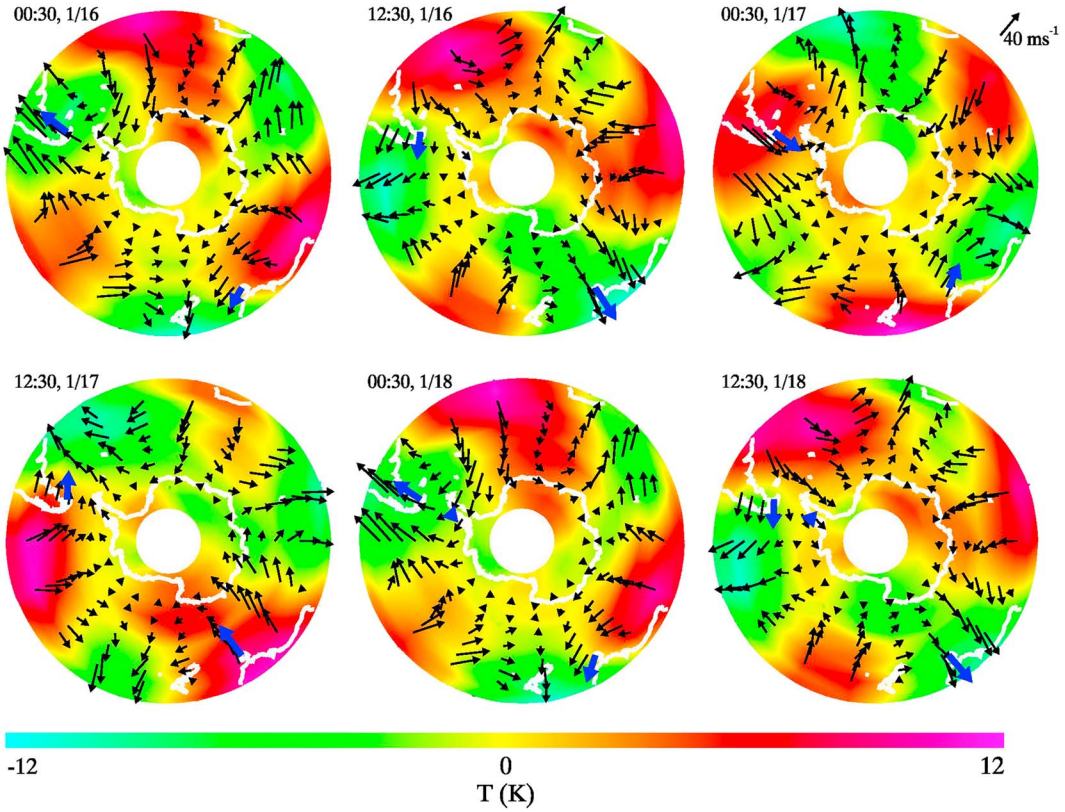

Figure 9. MLS Q2DW winds and temperatures from 30°S to 70°S at 91 km and 12-hr intervals spanning 1.25 cycles beginning at 00:30 on 16 January. Horizontal winds determined by meteor radars at Kingston, TdF, and Rothera are shown in blue for comparison. Note that S0 was removed from the temperature fields to avoid strong mean oscillations.

radars, by up to ~30% at most times, but with larger differences at times when radar or MLS amplitudes were changing rapidly, for example, the earlier times at TdF and Rothera. Finally, phase differences between radar and MLS estimates were quite small at most times, especially at times when amplitudes were nearly constant, but larger phase differences clearly accompanied the more rapid variations.

Influences of the Q2DW modal superposition on the intraperiod evolution are illustrated with a subset of the evolution shown in Figure 7 at a 12-hr cadence in Figure 9. These fields reveal strong variability in the full Q2DW field due to finite mode amplitudes having differing longitudinal wavenumbers, propagation directions, and phase speeds. Because all modes had approximately 48-hr periods, temporal differences of 48-hr yielded nearly identical images of the respective fields (e.g., first and fifth images and second and sixth images).

Different eastward or westward propagation among modes at 12-hr intervals yielded large changes in the locations of longitudinal maxima and minima of winds and T' on short time scales. At all times, W3 was dominant at lower latitudes because of its much larger amplitudes. But other modes contributed to strong suppression and/or augmentation of the W3 responses at specific longitudes at low and middle latitudes and dominated the Q2DW fields at high latitudes. For example, see the apparent eastward progression of the positive T' maximum initially at bottom at 00:30 on 17 January. Also, note the oscillating dominance of T' at high latitudes between zonal wavenumbers 1 and 2. Finally, while Movie S1 reveals largely clockwise rotation of the winds in the full Q2DW field, there are discrete locations at which counterclockwise rotations, or lack of a clear rotation, dominate the total response. These occur at the lower latitudes and are typically separated by ~60° of longitude, for example, east and west of South America, east of Africa, and west of Australia. They also have smaller amplitudes, suggesting that these are regions where other modes oppose W3 (see section 3.3).

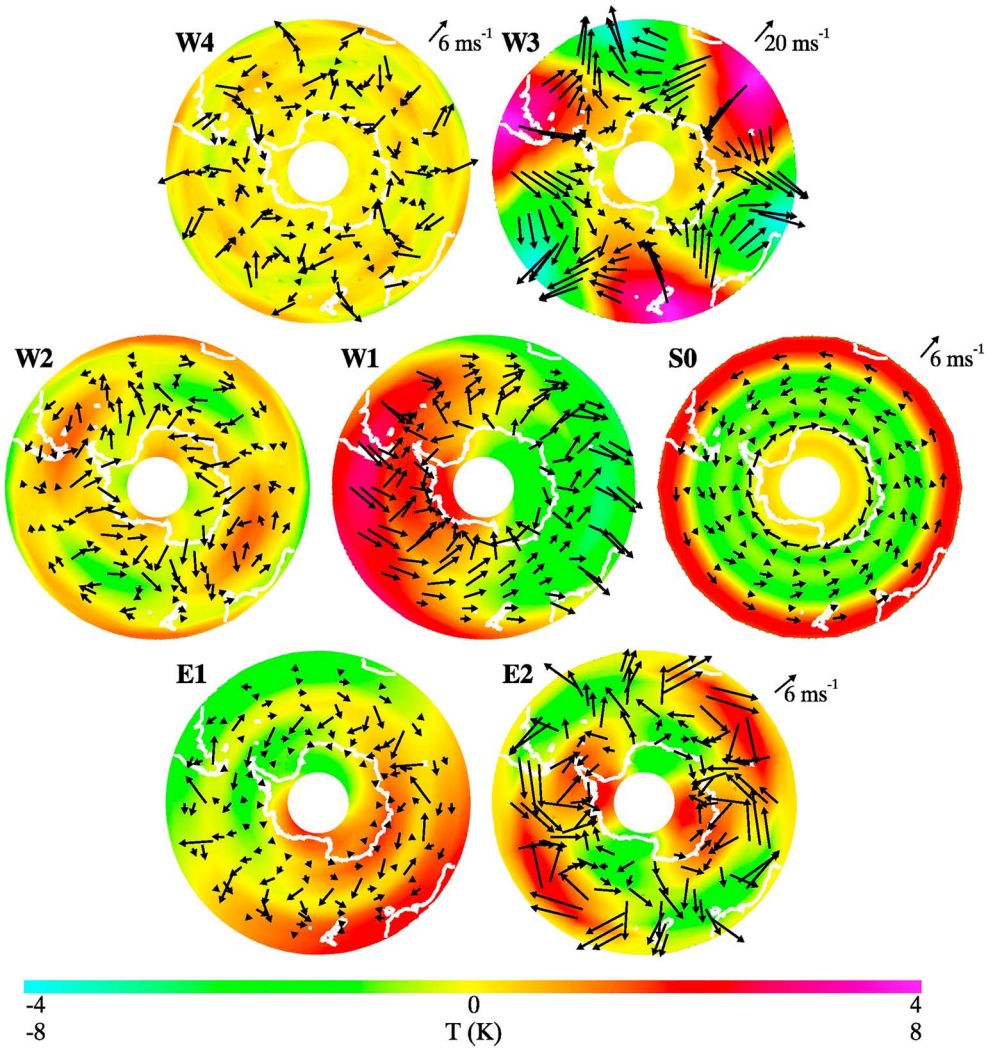

Figure 10. MLS Q2DW winds and temperatures from 30°S to 70°S at 91 km at 00:30 on 17 January for each mode.

3.3. MLS Q2DW modal decomposition

MLS definition of the evolving Q2DW u', v', and T' fields from middle to high latitudes also enabled decomposition of these fields into their various eastward and westward propagating and stationary components throughout the Q2DW evolution. This decomposition is shown at 00:30 UT at 91 km on 17 January in Figure 10 (also see Movie S2 in supporting information, which shows all but the weak E1 mode). The opposite phase of S0 is not shown but reveals significant eastward u' at the lowest latitudes. The modal decompositions are also shown in Figure 11 with u', v', and T' amplitudes as functions of latitude and time averaged from 81 to 97 km and in Figure 12 with u', v', and T' cross sections in latitude and altitude at 00:30 UT on 17 January.

As noted above, the full fields throughout the event were dominated by W3, which achieved u', v', and T' maxima at 91 km extending with large amplitudes to ~50°S but with amplitudes decreasing strongly poleward. Peak amplitudes at 91 km were ~25 and 50 m/s and ~10 K, respectively, at 45°S and were maintained to ~30°S in v' and T' (see larger color scales for W3 in Figures 11 and 12). Specific features of the various modal contributions include the following:

1. W1 achieved u' and v' maxima of ~8–10 m/s at ~45°S during the growth phase of W3 and T' maxima of ~3 K during the W3 peak;

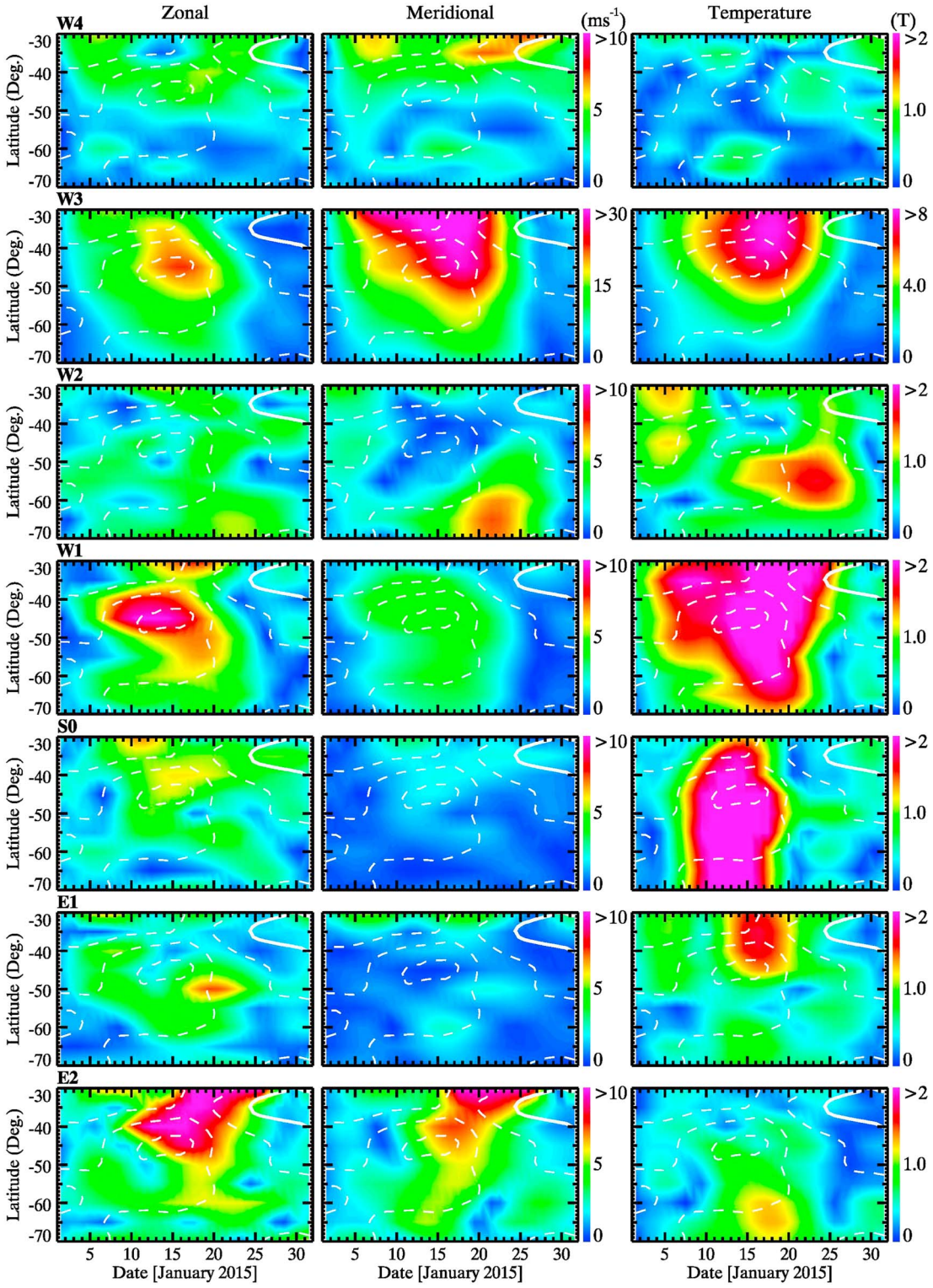

Figure 11. MLS amplitude variations (average of 81, 86, 91, and 97 km) of all Q2DW modes W1–W4 and E2 in u', v', and T' with latitude and time throughout this event. Note the different wind and T' color scales. Lines are zonal mean zonal wind, with solid eastward and dashed westward.

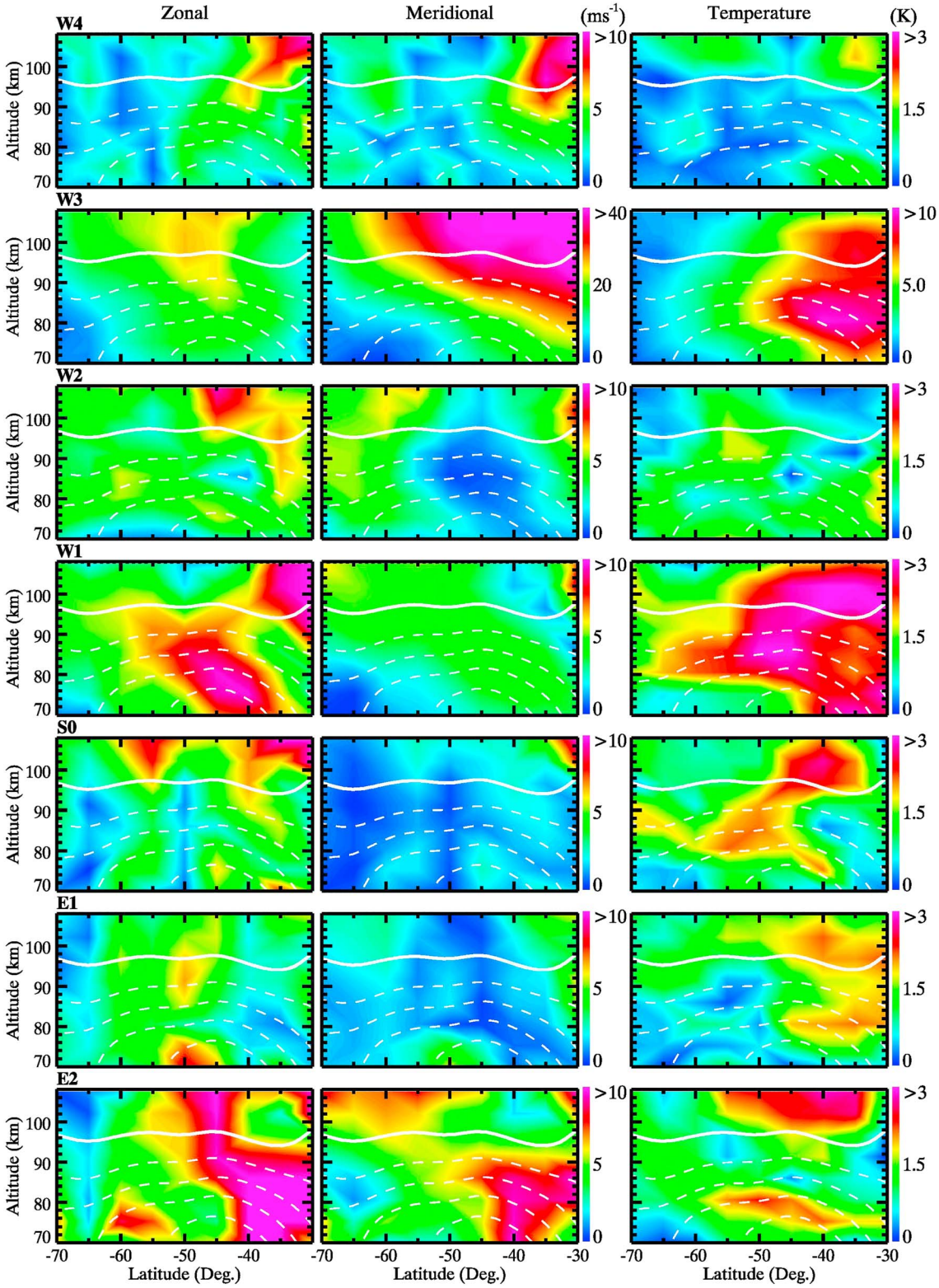

Figure 12. As in Figure 5, but for individual Q2DW mode amplitudes as functions of altitude and latitude on 17 January. The bold white line denotes $U = 0$ and solid (dashed) lines show positive (negative) U at 20-m/s intervals. Color scales for each row are shown at right of the center and right panels.

2. W2 achieved u' and v' maxima of ~6–8 m/s at 65°S and T' maxima of ~2 K at 55°S that trailed the W3 maxima;
3. W4 had u' and v' maxima of ~6–8 m/s at lower latitudes (though with significant variability) but only very small T' maxima at low to high latitudes that appear uncorrelated with W3 maxima;
4. E2 achieved u' and v' maxima of ~8–10 m/s at low and middle latitudes and T' maxima of ~1–2 K from middle to high latitudes accompanying the W3 peak;
5. E1 had weak and variable winds, except at ~50°S where u' maxima were ~6–8 m/s, and T' ~ 1–2 K maxima somewhat stronger at lower latitudes; and
6. S0 had in-phase u' ~ 8–10 and ~2–3 m/s at 30–40°S and 70°S, with an antiphase peak of ~2–3 m/s at middle latitudes and broad T' peaks of ~2 K from middle to high latitudes.

These fields also indicate more clearly where different modes were or were not able to contribute to observed Q2DW u', v', and T' fields; their spatial and temporal variability; and their phase variations in altitude at the various radars. Examples include the following:

1. W3 made the major contributions to radar winds at Adelaide and poleward but was likely not responsible for the major meridional response at CP seen in Figure 5;
2. W3 u' and v' roughly doubled from ~80 to 97 km, whereas T' peaked at ~85 km;
3. Only E2 and W4 could have contributed to the strong CP meridional response late in the event, assuming this was associated with a SH Q2DW;
4. Only E2 likely contributed to the local regions of opposite rotation of the full wind field during the peak Q2DW response from ~16 to 20 January;
5. W1, S0, and E2 likely contributed to the variable responses in time at Kingston and TdF;
6. Only W1, W2, W3, and E2 could have contributed to the steeper phases in u' and v' at Syowa and the anomalous phase variations in both wind components at Davis;
7. Only W1 and E2 contributed significantly to the T' fields at the highest latitudes;
8. W1 and E2 exhibited phase advances at low and middle latitudes when their T' were comparable to or exceeded those in W3 prior to ~10 January;
9. Phase advances in W3 at low latitudes, in W1 at low and high latitudes, and in E1 and E2 accompanied the peak event from ~16 to 20 January; and
10. Phase advances persisted at high latitudes in W1, E1, and E2 for ~1 cycle thereafter.

Various evidence above indicates that most of the Q2DW responses are consistent with a multimode SH event extending to Antarctic latitudes. However, the delayed peak v' amplitude at CP, the absence of a coincident CP u' peak, and the occurrence of clockwise wind rotations suggest an alternate explanation at low latitudes. To explore this further, Q2DW wind hodographs from 10 to 20 January are shown in Figure 13. These show the wind fields to have been counterclockwise at all sites where data were available, except at CP after ~13 January, when the wind field exhibited clear clockwise rotation. The implication is that the CP response was instead the southern extension of a NH event across the equator at these times.

3.4. Q2DW Vertical Structure at High Latitudes

Finally, we return to variations of Q2DW vertical phase structure and propagation with altitude. Figure 6 reveals downward phase progression, implied upward propagation, and inferred vertical wavelengths at MLT altitudes of λ_z ~ 75–100 km at Adelaide and Kingston, based on radar measurements of the superposed Q2DW modes at those sites. Even larger λ_z ~ 150–300 km is implied at TdF, while measured phases at Rothera suggest either very large λ_z or evanescence. Phases at Davis and Syowa, only slightly more poleward than Rothera, indicate phase ascent with time (apparent downward propagation) at both sites in u' and at Davis in v' and phase descent with time at Syowa in v'. It cannot be determined from the radar measurements alone whether these results are representative of the Q2DW field as a whole or whether they are biased by the Q2DW mode superposition, the mode variations in space and time, the period band-pass employed for the radar data analysis, or influences of other dynamics at large scales.

To resolve these uncertainties, we also assess the vertical structure for each Q2DW mode for the interval centered on the event peak on ~20 January at middle and high latitudes (see Figure 3). The balance wind u' and v' phase and amplitude profiles for each Q2DW mode at 70°S and 0°S longitude are shown in the top left and right panels of Figure 14 (see mode color legend in the upper left panel). These reveal that

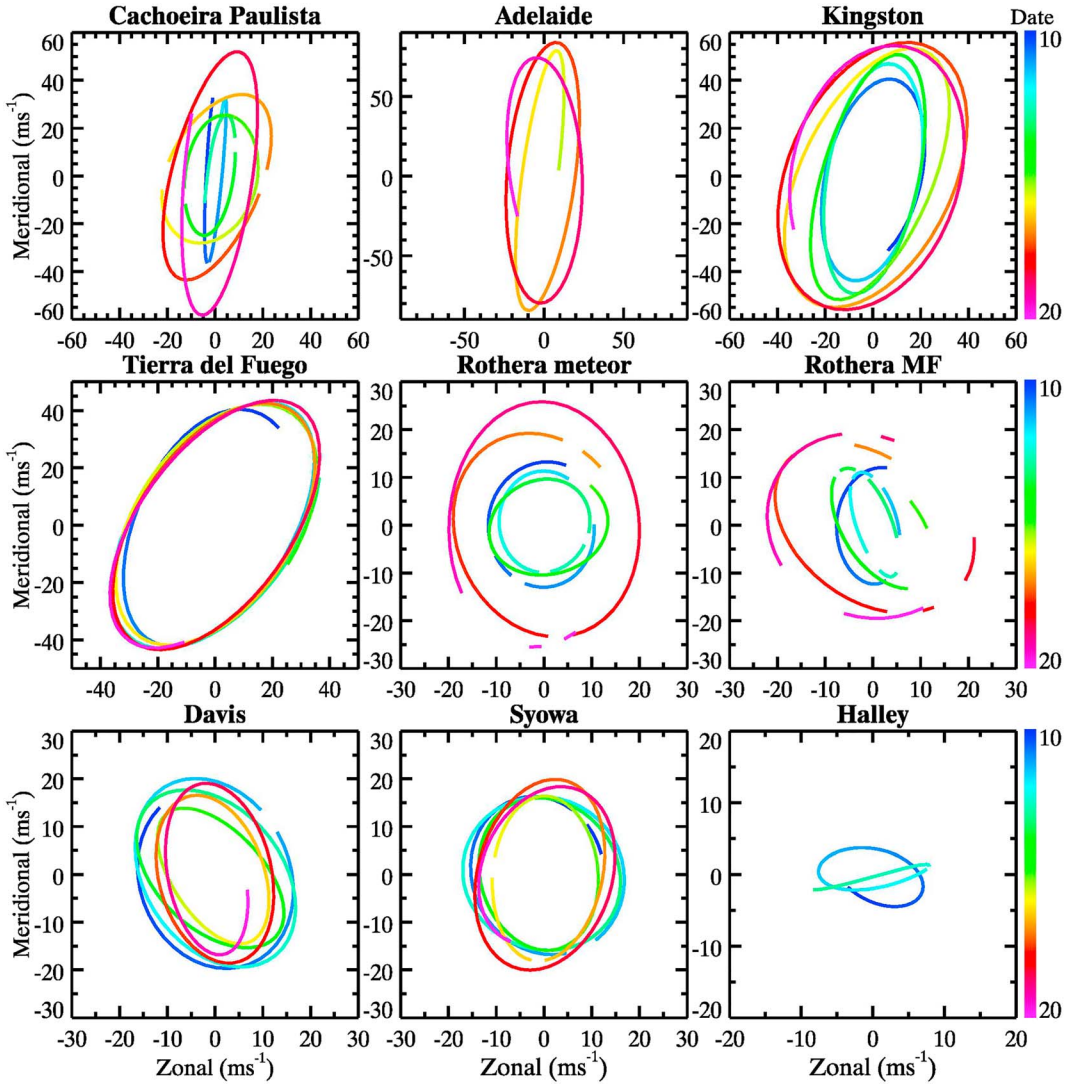

Figure 13. Radar Q2DW wind hodographs from 10 to 20 January at 90 km. Note the reversed rotation at CP at earlier times and larger amplitudes.

only W3, W2, and W1 have u' or v' larger than 5 m/s. The phases for each are also nearly vertical or suggest rapid upward phase progression in time.

Full balance wind phase and amplitude profiles at the locations of Rothera, Syowa, and Davis are compared with the radar profiles in the lower panels of Figure 14. These necessarily comprise primarily W3, W2, and W1. Additionally, the u' and v' magnitudes at Rothera, and for u' at Syowa, are comparable to or larger than those for W3 plus W2 alone. These results imply approximate phase alignments in these cases. In contrast, MLS balance wind u' and v' at Davis, and to a lesser extent v' at Syowa, suggest significant cancellation among the dominant Q2DW modes identified at these latitudes. In particular, the results at Syowa and Davis, which are separated by only 38° in longitude, have implied amplitude differences: those at Syowa are larger by ~2–3 times, and there are rapid, but different, implied phase progressions in the vertical with time at the two sites.

Turning to comparisons of the MLS balance winds and radar winds at these Antarctic sites, we see reasonably good comparisons in amplitudes and phases at Rothera, for example, amplitude differences of ~20% and phase differences of ~1–4 hr, that are consistent with those shown as time series at specific altitudes in Figure 8. Agreements between balance and radar winds at Davis and Syowa are not as compelling, but

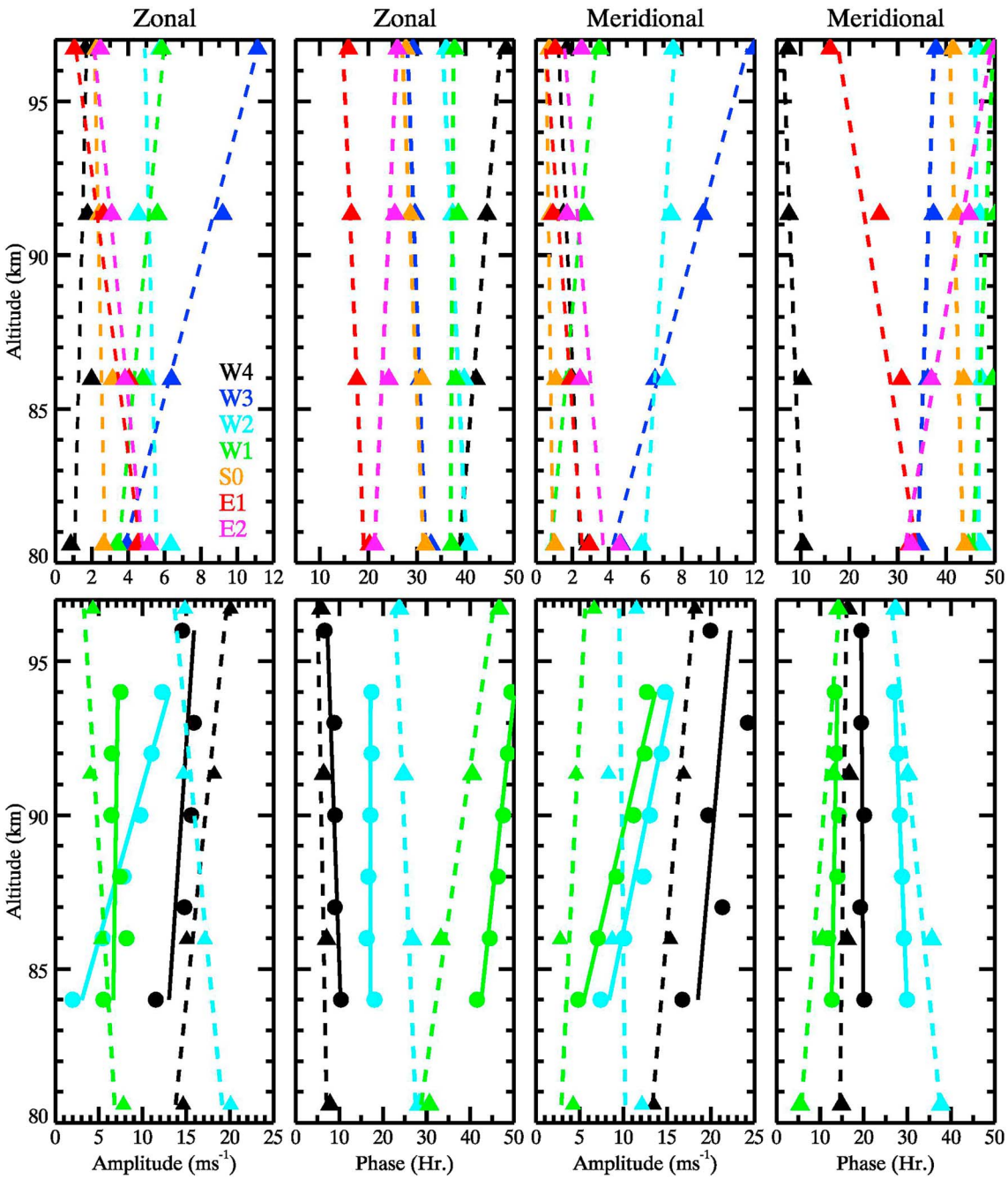

Figure 14. MLS balance wind amplitude and phase profiles for individual Q2DW modes (u' and v' at top left and right, respectively) at 70°S and as close to 0° longitude as possible. Full Q2DW balance wind and radar wind amplitude and phase comparisons near Rothera, Syowa, and Davis (u' and v' at bottom left and right, respectively. Q2DW mode color codes are shown in the top left panel. Radar color codes are as in Figure 5: Rothera, black; Syowa, light blue; and Davis, green.

they do exhibit good agreement in several cases. These include (1) u' ~ 5–7 m/s and meridional phase at Davis and (2) v' ~ 8–12 m/s and meridional phase at Syowa. Zonal and meridional amplitudes at Syowa and Davis, respectively, agreed only at the highest and lowest radar altitudes. In contrast, zonal phases at both sites differed by ~5–8 hr where radar amplitudes were small at both sites.

It is not surprising that agreement between MLS balance winds and radar winds is not uniformly good at high southern latitudes. Amplitude and phase estimates by both methods must be less confident when

amplitudes are small, as was the case for balance wind estimates of all but W3 and W2 at the higher altitudes. Additionally, 10-day means required to define the balance winds with asynoptic sampling surely masked variability of all of the Q2DW modes on shorter time scales and likely led to aliasing among the various modes contributing at these latitudes. While not a factor in our analysis, variability of other large-scale motions, such as tides and other PWs, spanning these time scales can in general contribute to the variable MLS fields and aliasing of inferred variances to other modes, with likely larger effects where Q2DW amplitudes are small.

3.5. MLS EP Fluxes, Divergence, and Zonal Mean Wind Accelerations

The polar summer MLT is the region of the atmosphere having a mean structure most dramatically impacted by systematic forcing by waves from below. GW momentum deposition drives a strong ageostrophic residual circulation comprising a meridional circulation from the summer to the winter mesopause of ~10–20 m/s at high summer latitudes (Nastrom et al., 1982), closure of the mesospheric jets in both hemispheres, and strong upwelling at high summer latitudes that yields a mean T ~ 130 K (McIntyre, 1989). GW momentum fluxes and implied drag accounting for these influences are $< u'w' >$~3–10 m^2/s^2 and D_x ~ 30–100 m/s/day poleward of ~30° (Luo et al., 1995; Richter et al., 2010). This is the environment in which the Q2DW evolves and with which its EP fluxes and induced mean influences at higher latitudes must be compared in understanding the impacts of specific events.

The component and total Q2DW fields described above enabled evaluation of the individual EP flux terms in equations (7) and (8). Of the Q2DW fluxes, the dominant terms were $< u'v' >$ in F^{ϕ} and $f< v'\theta' >/(\partial\theta_0/dz)$ in F^z, each weighted by $\rho_0 a \cos\phi$. To examine relative EP flux contributions by the Q2DW and the GW $<u'w'>$ in F^z, altitude-time cross sections of the dominant Q2DW terms are shown at 35°S, 45°S, 55°S, and 65°S in Figure 15. Both terms are significantly larger than the other Q2DW contributions to the component fluxes.

Q2DW contributions to F^{ϕ} (Figure 15, left panels) achieve maxima decreasing from ~250 m^2/s^2 at 35°S to ~80 m^2/s^2 at 65°S. These exhibit earlier maxima at lower latitudes that can only have been contributed by the W3, W1, and E2 modes (see Figures 11 and 12 and the discussion in section 3.3). Q2DW contributions to F^z (Figure 15, right panels) achieve maxima of ~2–3 m^2/s^2 at 35–45°S and decreasing magnitudes at higher latitudes. The maxima in these fields occur from ~17 to 20 January and are coincident with those in F^{ϕ} at from 45°S to 65°S.

These vertical Q2DW EP fluxes, F^z, are somewhat smaller than the limited ground-based measurements of GW $<u'w'>$ ~ 3–10 m^2/s^2 or larger at comparable northern and southern latitudes (de Wit et al., 2017; Fritts & Yuan, 1989; Placke et al., 2011, 2015; Wang & Fritts, 1990). If the GW and Q2DW vertical EP fluxes have roughly comparable vertical gradients, as suggested by the observations and modeling cited above, they would imply somewhat smaller Q2DW influences on their environment at these times. The relative contributions of F^{ϕ} and F^z to Q2DW EP flux divergence and their implications for the Q2DW environment are described below.

EP flux vectors and the divergence of EP flux per unit mass (zonal acceleration) were computed from the observed and inferred MLS fields employing equations (7) and (8) and 10-day asynoptic sampling separately for each Q2DW mode. These fields are shown in Figure 16 centered on 12, 17, and 22 January in order to illustrate their evolution spanning the peak of the Q2DW event. A movie of these fields at higher temporal resolution is provided for reference (see Movie S3 in the supporting information). Q2DW EP flux vectors were normalized as described by Lieberman (1999, 2002). The dominant contributions for W3 and the full field were the horizontal momentum fluxes, $-< u'v' >$, in equation (7) and the Coriolis term in equation (8). The first term at right in equation (7) nevertheless made a somewhat weaker opposing contribution centered at ~86 km near the event peak in time. Note that the color scale and the EP flux vector maxima are 5 times larger for W3 than for all other modes.

Considering first the dominant W3 fields, we see a large region of eastward accelerations centered at ~75- to 85-km altitudes and ~40–50°S latitudes spanning this interval, with the larger accelerations at the two earlier times. A corresponding large region of deceleration is seen on 12 January extending from ~80 to 85 km to above 107 km and from ~30°S to 55°S, with the major decelerations confined to the higher altitudes and lower latitudes but a weaker, secondary maximum centered at ~95 km and ~50°S. The region of stronger

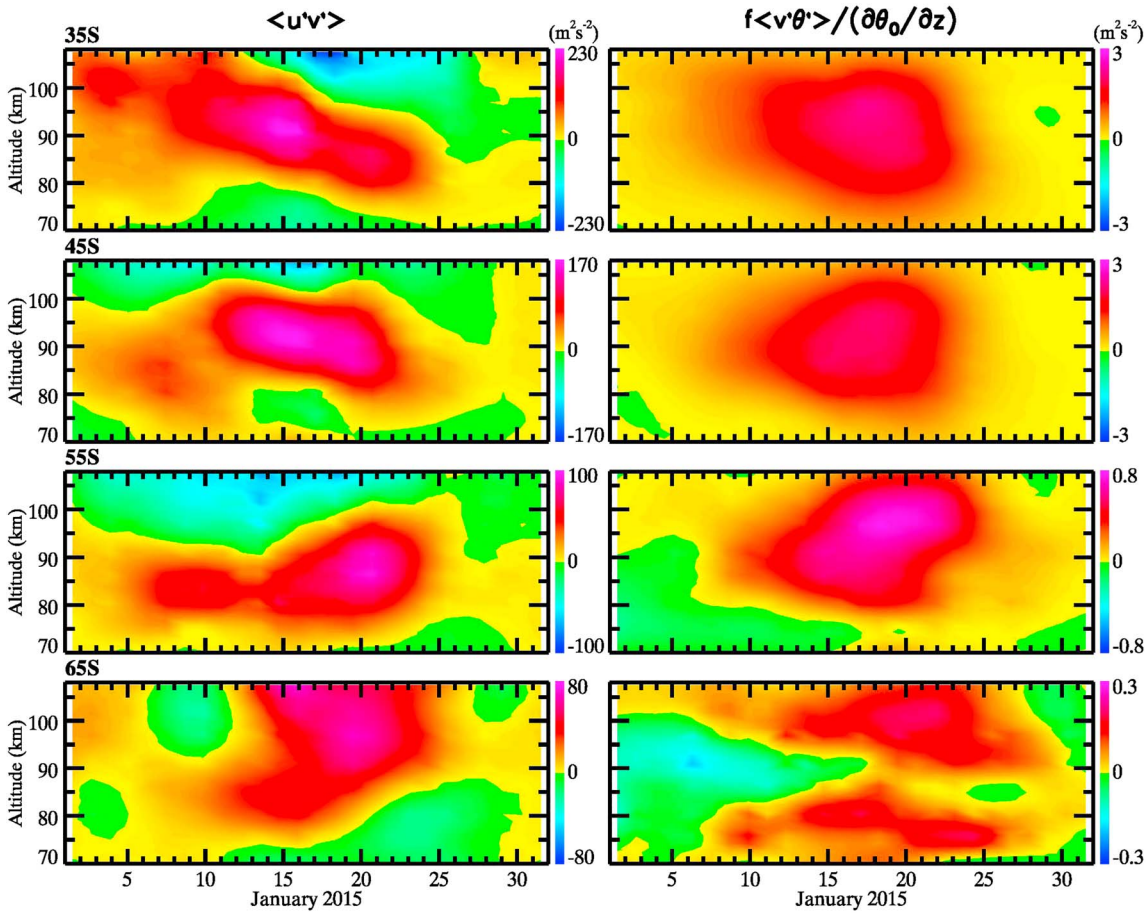

Figure 15. Altitude-time cross sections of Q2DW (left and right) $< u'v' >$ in F^{ϕ} and $f < v'\theta' > /(\partial\theta_0/\mathrm{d}z)$ in F^{z} at (top to bottom) 35°S, 45°S, 55°S, and 65°S. Note the different color scales in each panel.

deceleration intensified and shifted to lower latitudes at later times, while the weaker region remained similar at 17 January and weakened thereafter.

The EP flux vectors exhibit increasing (decreasing) upward fluxes below (above) ~90 km at each time but shifting from southward on 12 and 17 January during the event intensification to northward on 22 January. The horizontal vector orientations on 12 and 17 January are also consistent with the Q2DW radar wind hodographs at Kingston and TdF at these times. Finally, the overall accelerations (decelerations) below (above) ~90 km act to reduce $\mathrm{d}U/\mathrm{d}z$, suggesting a largely baroclinic source of the Q2DW at these times.

Other Q2DW modes also exhibited coherent responses, EP fluxes, and implied accelerations accompanying the W3 response at these times, though with generally smaller influences on the zonal flow. The most prominent and consistent of these were by W2, W1, and E2. The W1 response most closely paralleled W3 in its occurrence in latitude and time, with similar EP flux and acceleration spatial patterns at middle latitudes at the earlier times, and at lower altitudes extending throughout the event. The similar initial evolutions suggest common source dynamics for the W1 and W3 modes.

W2 exhibited major responses poleward of the W3 response that began at higher altitudes, shifted to lower altitudes and increased throughout this interval, and were strongest as W3 was weakening. E2 exhibited responses similar to, but also poleward of, W3 at lower altitudes and largely opposite to those of W3 at lower latitudes and higher altitudes. Stronger EP flux modulation in latitude for E2 than seen for the other modes yielded more strongly modulated mean zonal accelerations as well. The differences in the W2 and E2 responses relative to W3 suggest different, higher-latitude SH source conditions than for W3 but potentially common sources for these modes.

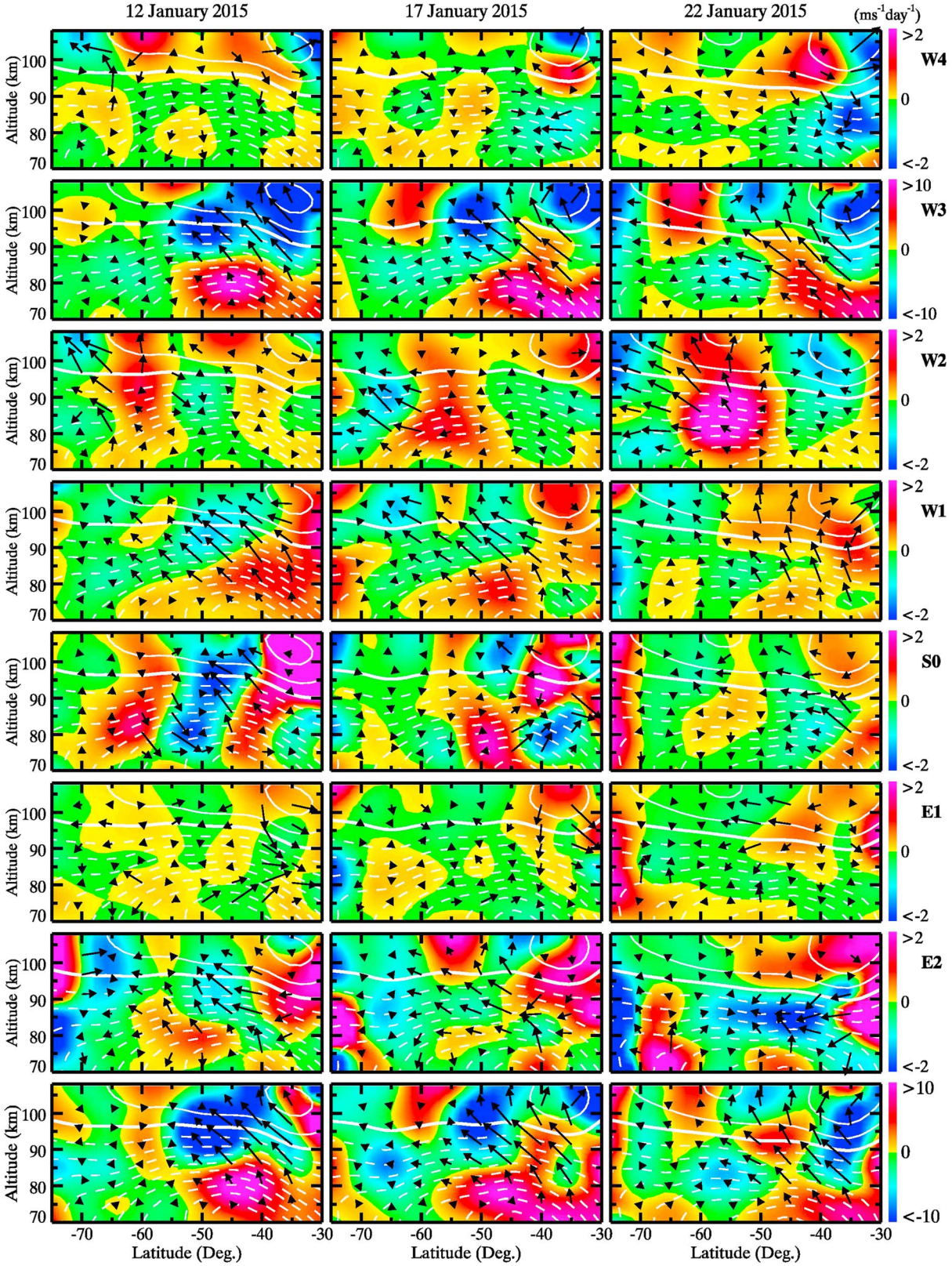

Figure 16. As in Figure 11 but for zonal tendencies implied by EP flux convergence for 10-day fits centered on 12, 17, and 22 January. Shown at the bottom are the cumulative fields including all Q2DW modes. Vectors show total EP fluxes, with horizontal and vertical length scales of 3 $m^2 \cdot s^{-2} \cdot degree^{-1}$ and 0.027 $m^2 \cdot s^{-2} \cdot km^{-1}$, respectively.

Both E2 and W2 also exhibited strong responses in u' and v' at lower latitudes at middle and higher altitudes throughout the event, but these were suggested above to accompany a NH event, given the opposite rotation of the wind field at these later times. By comparison with the modes discussed above, E1, S0, and W4 had weak wind responses except at higher altitudes and lower latitudes, and all other responses were small in comparison to W3.

Finally, we evaluated the contributions of W3 and the full Q2DW to EP flux divergences near the mesopause at high latitudes on 12, 17, and 22 January. Horizontal divergences of F^{Φ} were somewhat larger than vertical divergences of F^{z} for W3, but the other modes significantly enhanced the divergence of F^{Φ} relative to F^{z}.

3.6. Evolutions of Mean *U*, *V*, *T*, and Φ Fields

Q2DW EP flux divergence at early and middle stages of the evolution (lower left and middle panels of Figure 16) imply a weakening of dU/dz from ~80 to 100 km at latitudes of ~40–55°, consistent with a primarily baroclinic instability source of the Q2DW event. At these same times, negative EP flux divergence at ~80–90 km and ~60–70° latitudes implies increasing westward U at these locations. These zonal wind tendencies opposed the expected GW forcing attributed with closing the mesospheric jet and suggest a weakening of the residual circulation balancing the ageostrophic zonal mean motion. Also, note that the higher-latitude forcing was due primarily to W3 but that E2, and to lesser degrees W1 and W2, also contributed to these responses. Together, these amounted to westward forcing of ~5 and 10 m/s/day on 12 and 17 January and weakening by 22 January.

To explore the consequences of EP flux divergence further, zonal mean wind tendencies computed from radar and MLS measurements at latitudes from ~45°S to 70°S are shown from 5 to 25 January at left and right, respectively, from top to bottom in Figure 17. Radar wind estimates employed a low-pass filter with a 6-day cutoff; MLS winds employed 10-day asynoptic sampling.

These fields exhibit quite good, perhaps even surprising, agreement overall, given the spatial and temporal variability of the individual Q2DW modes throughout this event and the very different local and global assessments of these fields. Both reveal much weaker dU/dt than implied by EP flux divergence and suggest instead a significant impact on the mean meridional circulation V and associated T.

MLS measurements of mean T from 81 to 96 km at 55°S, 65°S, 70°S, and 75°S are shown from 1 December 2014 to 28 February 2015 in the upper four panels of Figure 18 (note the decreasing color scales with increasing latitudes). The maximum mean T on 17 January at 81 km and 55°S, 65°S, 70°S, and 75°S were 177, 166, 163, and 159 K, respectively, thus ~5 and 10 K warmer than ~10 days earlier and later. The implications of these fields are that the Q2DW EP flux divergence seen at high latitudes and ~80–90 km in Figure 16 induced westward zonal mean accelerations that were responsible for a transient weakening of the high-latitude residual circulation, a reduction in the adiabatic cooling accompanying upwelling, and a corresponding increase in the mean T at these altitudes and latitudes in response to transient Q2DW forcing. For reference, this transient mean T maximum is within a broader summer minimum and PMC maximum typically centered ~10 days earlier. The rapid rise in MLS $T(z)$ beginning 20 days later is consistent with previous observations of these dynamics during SH and NH polar summer and modeling of the relevant dynamical and radiative influences (France et al., 2018; Lübken et al., 2004; Luo et al., 1995). Finally, we note that the Q2DW westward forcing during this event was roughly 10% of the expected GW forcing accounting for the cold summer mesopause and that the induced changes in T by the Q2DW appears to have been roughly proportional to that due to the mean GW forcing.

4. Discussion

Our analysis of the SH January 2015 Q2DW event using both radar and MLS measurements has confirmed a number of previous findings and yielded several new results. The dominant Q2DW period was ~46 hr during the major response, u' and v' amplitudes were as large as 35 and 55 m/s, respectively, and T' achieved a maximum of ~12 K. These amplitudes were comparable to or somewhat weaker than previous SH Q2DW events. Specifically, they were weaker than those in 2011, 2012, and 2014 based on radar measurements at TdF (not shown), which likewise exhibited transient PMC reductions (C. Randall, personal communication, 2018). Our joint radar and MLS analysis also revealed W3 to be the dominant mode but with additional responses in W1, W2, W4, S0, E1, and E2, several of which were previously identified by various authors (Limpasuvan

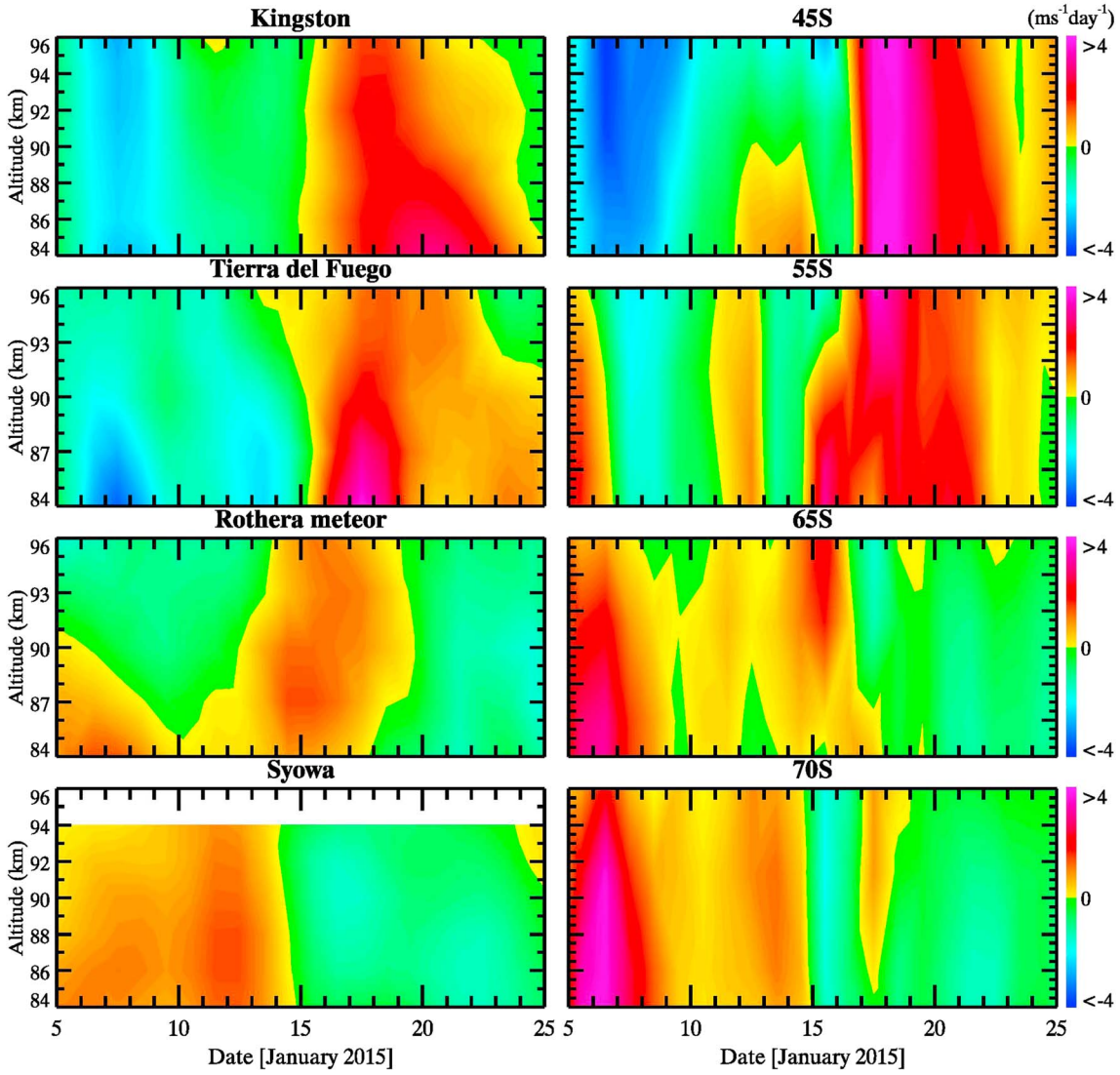

Figure 17. Zonal mean wind tendencies computed at radar sites from 6-day low-passed radar winds (left column) and for the 10-day mean contributions from MLS balance wind estimates (right column) from 45°S to 70°S.

& Wu, 2009; Meek et al., 1996; Merzlyakov et al., 2004; Morris et al., 2009; Pancheva et al., 2004; Sandford et al., 2008; Tunbridge et al., 2011). In the January 2015 event, W3 had u', v', and T' amplitudes ~3–10 times larger than all other modes of which E2 had the largest amplitudes.

A number of previous studies addressed the generation of the Q2DW E2 component via the nonlinear interaction of the Q2DW W3 mode and DW1 (Forbes & Moudden, 2012; Lieberman et al., 2017; McCormack et al., 2010; Moudden & Forbes, 2014; Nguyen et al., 2016). Our results provide additional evidence of this expected Q2DW E2 source, given the coincidence of the W3 and E2 responses in time, the simultaneous occurrence of a large-amplitude DW1 at MLT altitudes (see the lower panels of Figure 18), and the apparent larger E2 responses than in other modes except W3 (especially in T') at altitudes above ~80 km and higher latitudes, as inferred from SABER observations by Nguyen et al. (2016) for the January 2006 event.

France et al. (2018) examined the roles of interhemispheric coupling and Q2DW responses in the 2014 NH summer. They argued that the local Q2DW response played the major role and demonstrated a transient warming and PMC reduction that were strongly correlated and very similar to the responses seen in our study.

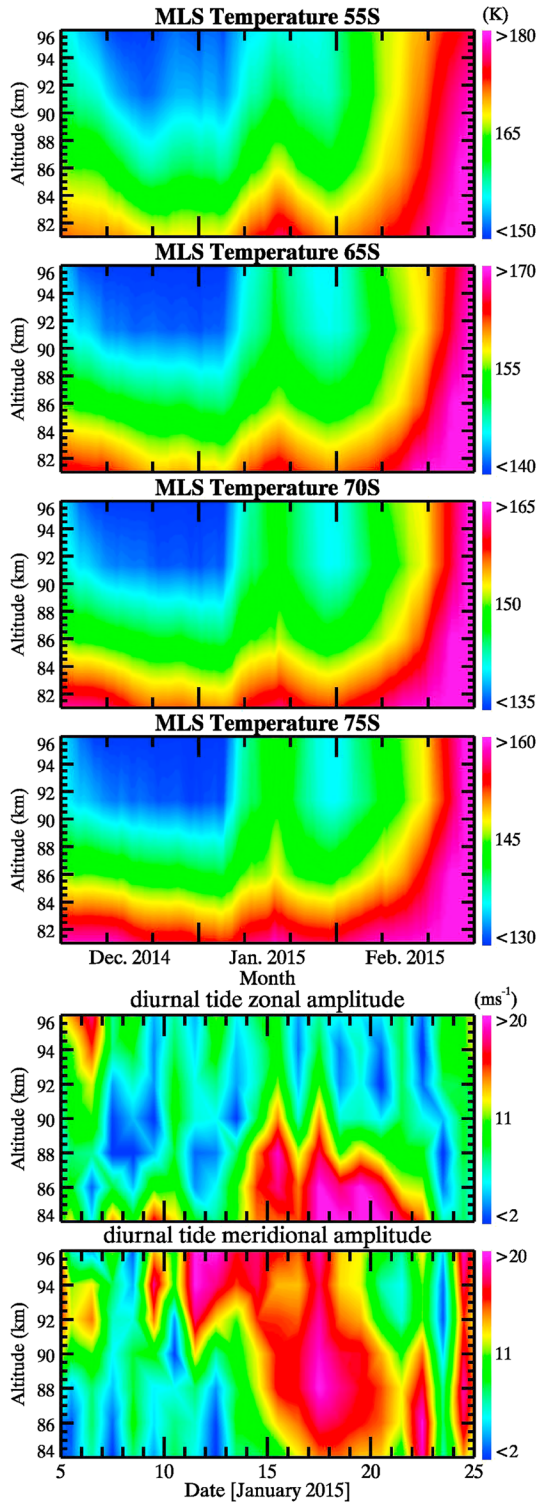

Figure 18. MLS mean $T(z,t)$ from 81 to 96 km and 1 December to 28 February 2018 at 55°S, 65°S, 70°S, and 75°S (top four panels, also note different color scales for each). Lower two panels show the diurnal tide zonal and meridional amplitudes from the Kingston meteor radar for the same period. Note the coincidence of the diurnal tide with the Q2DW E2 mode centered at ~15–20 January in Figure 10.

Additional results of our analyses not addressed in previous studies include the following:

1. Weaker responses having shorter periods at earlier times at middle to higher latitudes,
2. Close agreement of radar and inferred balance equation winds using MLS in the MLT,
3. An implication of credible/verified Q2DW mean flow responses from averaged MLS data,
4. Quantified individual Q2DW modes and their EP fluxes, including S0 not previously identified in other analyses,
5. W1 and S0 maxima accompanying increasing W3 amplitudes,
6. W2 and W4 maxima accompanying decreasing W3 amplitudes, and
7. An E1 maximum accompanying the W3 maximum.

We have no explanation at present for the shorter periods and initial W1 and S0 responses at earlier times, nor for the delayed responses of W2 and W4 relative to the W3 peak response. The timing and mix of the various Q2DW modes could be dictated by longitudinal variability of the expected baroclinic instability source strength. But this cannot be inferred from these data, and modeling of such sources may be required to explain these or similar observations. However, the close agreement between the radar and MLS definitions of the Q2DW wind amplitudes and phases throughout this event suggests that we can have some confidence in the modal decomposition, their spatial and temporal variability, and their EP fluxes and divergence. In particular, our analysis appears to provide the first evidence of the Q2DW S0 mode and its contributions to the EP fluxes and mean flow forcing.

EP flux divergence by the full Q2DW and individually by W3 suggests a largely baroclinic source at midlatitudes during the growth phase of this event (see Figure 16 at 12 and 17 January). This, the weakening of the residual circulation near the polar mesopause, and the accompanying transient warming during the strongest response are again consistent with the findings of France et al. (2018) for the July–August 2014 NH Q2DW event and with the simple numerical model of Lieberman (1999) employed in that study. Our results likewise coincided with a strong transient PMC reduction at SH polar latitudes during January 2015 (C. Randall, personal communication, 2018).

5. Summary and Conclusions

We have performed an analysis of the January 2015 SH Q2DW event using MLT radar winds from ~23°S to 76°S and MLS temperature and geopotential height measurements from ~30°S to 75°S. Balance winds including the tendency terms were obtained using the asynoptic sampling method for running 10-day intervals. The full balance wind response was found to agree well with radar winds determined for running 10-day intervals at midlatitudes where amplitudes were large. This agreement suggested confidence in the balance winds of individual Q2DW modes and their EP fluxes and divergence.

Our assessment of the Q2DW modes revealed the expected dominance of the full response by the W3 mode, with measureable amplitudes in westward modes W1, W2, and W4, eastward modes E1 and E2, and the first inference of a stationary Q2DW response, S0. Of these secondary modes, E2 and S0 contributed most at midlatitudes, whereas E2 and W1

enhanced the forcing by W3 at lower altitudes and higher latitudes. The consequences were a suppressed residual mean circulation, increased mean temperature and geopotential height, and reduced intensities of PMCs in the upper mesosphere accompanying this event. Finally, our results support the conclusions of earlier studies that E2 arises from the nonlinear interaction of the dominant W3 mode and DW1, given the coincidence of E2 with W3 and a strong DW1 at midlatitudes as the event develops.

Acknowledgments
Research described here was funded by NSF and NASA grants cited in GEMS. The Kingston meteor radar was funded by Atrad Pty Ltd and supported by AAS grant project 2668. The Adelaide meteor radar is supported by Atrad Pty Ltd and the University of Adelaide. Operation of the Davis and Kingston radars was supported through Australian Antarctic Science project 4025. The Rothera MF radar is a joint project between GATS and the British Antarctic Survey (BAS). The Rothera meteor radar is a joint project between the University of Bath and BAS. The Halley MF radar is operated by BAS. Andrew J. Kavanagh is supported by the Natural Environment Research Council, National Capability (NE/R016038/1). Movies showing the evolutions of the full Q2DW field and the individual Q2DW components throughout this event are provided as supporting information (see Movies S1–S3). The authors are indebted to Genesis staff in Adelaide, Australia and Estacion Astronomica Rio Grande staff in Rio Grande, Argentina, for their efforts in maintaining SAAMER. MLT radar data used here are available online (https://cedarweb.vsp.ucar.edu/wiki/index.php/Data_Services:Main). MLS data are available online (https://mls.nasa.gov/data?).

References

Andrews, D. G., Holton, J. R., & Leovy, C. B. (1987). *Middle Atmosphere Dynamics* (1st ed.). San Diego, CA: Academic Press.

Azeem, S. M. I., Palo, S. E., Wu, D. L., & Froidevaux, L. (2001). Observations of the 2-Day wave in UARS MLS temperature and ozone measurements. *Geophysical Research Letters*, *28*(16), 3147–3150. https://doi.org/10.1029/2001GL013119

Baumgaertner, A. J. G., McDonald, A. J., Hibbins, R. E., Fritts, D. C., Murphy, D. J., & Vincent, R. A. (2008). Short-period planetary waves in the Antarctic middle atmosphere. *Journal of Atmospheric and Solar - Terrestrial Physics*, *70*(10), 1336–1350. https://doi.org/10.1016/j.jastp.2008.04.007

Clark, R. R., Currnet, A. C., Manson, A. H., Meek, C. E., Avery, S. K., Palo, S. E., & Aso, T. (1994). Hemispheric properties of the two-day wave from mesosphere-lower thermosphere radar observations. *Journal of Atmospheric and Terrestrial Physics*, *56*(10), 1279–1288. https://doi.org/10.1016/0021-9169(94)90066-3

de Wit, R. J., Janches, D., Fritts, D. C., Stockwell, R. G., & Coy, L. (2017). Unexpected climatological behavior of MLT gravity wave momentum flux in the lee of the Southern Andes hot spot. *Geophysical Research Letters*, *44*, 1182–1191. https://doi.org/10.1002/2016GL072311

Ern, M., Preusse, P., Kalisch, S., Kaufmann, M., & Riese, M. (2013). Role of gravity wave in the forcing of quasi two-day waves in the mesosphere: An observational study. *Journal of Geophysical Research: Atmospheres*, *118*, 3467–3485. https://doi.org/10.1029/2012JD018208

Forbes, J. M., & Moudden, Y. (2012). Quasi-two-day wave-tide interactions as revealed in satellite observations. *Journal of Geophysical Research*, *117*, D12110. https://doi.org/10.1029/2011JD017114

France, J. A., Randall, C. E., Lieberman, R. S., Harvey, V. L., Eckermann, S. D., Siskind, D. E., et al. (2018). Local and remote planetary wave effects on polar mesospheric clouds in the Northern Hemisphere in 2014. *Journal of Geophysical Research: Atmospheres*, *123*, 5149–5162. https://doi.org/10.1029/2017JD028224

Fritts, D. C., & Alexander, M. J. (2003). Gravity wave dynamics and effects in the middle atmosphere. *Reviews of Geophysics*, *41*(1), 1003. https://doi.org/10.1029/2001RG000106

Fritts, D. C., Iimura, H., Lieberman, R., Janches, D., & Singer, W. (2012). A conjugate study of mean winds and planetary waves employing enhanced meteor radars at Rio Grande, Argentina (53.8°S) and Juliusruh, Germany (54.6°N). *Journal of Geophysical Research*, *117*, D05117. https://doi.org/10.1029/2011JD016305

Fritts, D. C., & Isler, J. R. (1994). Mean motions and tidal and two-day structures and variability in the mesosphere and lower thermosphere over Hawaii. *Journal of the Atmospheric Sciences*, *51*(14), 2145–2164. https://doi.org/10.1175/1520-0469(1994)051<2145:MMATAT>2.0.CO;2

Fritts, D. C., Isler, J. R., Lieberman, R. S., Marsh, M. D., Nakamura, T., Tsuda, T., et al. (1999). Two-day wave structure and mean flow interactions observed by radar and High Resolution Doppler Imager. *Journal of Geophysical Research*, *104*(D4), 3953–3969. https://doi.org/10.1029/1998JD200024

Fritts, D. C., & Yuan, L. (1989). Measurement of momentum fluxes near the summer mesopause at Poker Flat, Alaska. *Journal of the Atmospheric Sciences*, *46*(16), 2569–2579. https://doi.org/10.1175/1520-0469(1989)046<2569:MOMFNT>2.0.CO;2

Froehlich, K., Pogoreltsev, A., & Jacobi, Ch. (2003). Numerical simulation of tides, Rosby and Kelvin waves with the COMMA-LIM model. *Advances in Space Research*, *32*(5), 863–868. https://doi.org/10.1016/S0273-1177(03)00416-2

Garcia, R. R., Lieberman, R., Russell, J. M. III, & Mlynczak, M. G. (2005). Large-scale waves in the mesosphere and lower thermosphere observed by SABER. *Journal of the Atmospheric Sciences*, *62*(12), 4384–4399. https://doi.org/10.1175/JAS3612.1

Glass, M., Fellous, J., Massebeuf, M., Spizzichina, A., Lysenko, I., & Portniaghin, Y. (1975). Comparison and interpretation of the results of simultaneous wind measurements in the lower thermosphere at Garchy (France) and Obnisnsk (USSR) by meteor radar technique. *Journal of Atmospheric and Terrestrial Physics*, *37*, 1077–1087.

Gu, S.-Y., Li, T., Dou, X., Wang, N.-N., Riggin, D. M., & Fritts, D. C. (2013). Long-term observations of the quasi two-day wave by the Hawaii MF radar. *Journal of Geophysical Research: Space Physics*, *118*, 7886–7894. https://doi.org/10.1002/2013JA018858

Gu, S.-Y., Li, T., Dou, X., Wu, Q., Mlynczak, M. G., & Russell, J. M. III (2013). Observations of Quasi-Two-Day wave by TIMED/SABER and TIMED/TIDI. *Journal of Geophysical Research: Atmospheres*, *118*, 1624–1639. https://doi.org/10.1002/jgrd.50191

Hagan, M. E., Forbes, J. M., & Vial, F. (1993). Numerical investigation of the propagation of the quasi-two-day wave into the lower thermosphere. *Journal of Geophysical Research*, *98*(D12), 23,193–23,205. https://doi.org/10.1029/93JD02779

Hecht, J. H., Walterscheid, R. L., Gelinas, L. J., Vincent, R. A., Reid, I. M., & Woithe, J. M. (2010). Observations of the phase-locked 2 day wave over the Australian sector using medium-frequency radar and airglow data. *Journal of Geophysical Research*, *115*, D16115. https://doi.org/10.1029/2009JD013772

Hitchman, M. H., & Leovy, C. B. (1987). Evolution of the zonal mean state in the equatorial middle atmosphere during October 1978 – May 1979. *Journal of the Atmospheric Sciences*, *43*, 3159–3176.

Hitchman, M. H., Leovy, C. B., Gille, J. C., & Bailey, P. L. (1987). Quasi-stationary zonally asymmetric circulations in the equatorial middle atmosphere. *Journal of the Atmospheric Sciences*, *44*(16), 2219–2236. https://doi.org/10.1175/1520-0469(1987)044<2219:QSZACI>2.0.CO;2

Huang, Y. Y., Zhang, S. D., Yi, F., Huang, C. M., Huang, K. M., Gan, Q., & Gong, Y. (2013). Global climatological variability of quasi-two-day waves revealed by TIMED/SABER observations. *Annales de Geophysique*, *31*(6), 1061–1075. https://doi.org/10.5194/angeo-31-1061-2013

Hunt, B. G. (1981). The 2-day wave in the middle atmosphere as simulated in a general circulation model extending from the surface to 100 km. *Journal of Atmospheric and Terrestrial Physics*, *43*(11), 1143–1154. https://doi.org/10.1016/0021-9169(81)90030-1

Iimura, I., Fritts, D. C., Janches, D., Singer, W., & Mitchell, N. J. (2015). Interhemispheric structure and variability of the 5-day planetary wave from meteor radar wind measurements. *Annales de Geophysique*, *33*(11), 1349–1359. https://doi.org/10.5194/angeo-33-1349-2015

Jacobi, C., Fröhlich, K., & Pogoreltsev, A. (2006). Quai two-day-wave modulation of gravity wave flux and consequences for the planetary wave propagation in a simple circulation model. *Journal of Atmospheric and Solar - Terrestrial Physics*, *68*(3-5), 283–292. https://doi.org/10.1016/j.jastp.2005.01.017

Kashcheyev, B. L., & Oleynikov, A. N. (1999). Radio investigation of spatial structure of the quasi 2-day wind velocity oscillations in the region of mesopause and lower thermosphere. *Telecommunications and Radio Engineering*, *53*(7-8), 24–29. https://doi.org/10.1615/TelcomRadEng.v53.i7-8.50

Lieberman, R. S. (1999). Eliassen-Palm fluxes of the 2-day wave. *Journal of the Atmospheric Sciences*, *56*(16), 2846–2861. https://doi.org/10.1175/1520-0469(1999)056<2846:EPFOTD>2.0.CO;2

Lieberman, R. S. (2002). Eliassen-Palm fluxes of the two-day wave, 2846-2861. *Corrigendum*, *59*, 2625–2627.

Lieberman, R. S., Akmaev, R. A., Fuller-Rowell, T. J., & Doornbos, E. (2013). Thermospheric zonal mean winds and tides revealed by CHAMP. *Geophysical Research Letters*, *40*, 2439–2443. https://doi.org/10.1002/grl.50481

Lieberman, R. S., Riggin, D. M., Nguyen, V., Palo, S. E., Siskind, D. E., Mitchell, N. J., et al. (2017). Global observations of 2 day wave coupling to the diurnal tide in a high-altitude forecast-assimilation system. *Journal of Geophysical Research: Atmospheres*, *122*, 4135–4149. https://doi.org/10.1002/2016JD025144

Lilienthal, F., & Jacobi, C. (2015). Meteor radar quasi-2-day wave observations over 10 years at Collm (51.3°N, 13.0°E). *Atmospheric Chemistry and Physics*, *15*(17), 9917–9927. https://doi.org/10.5194/acp-15-9917-2015

Limpasuvan, V., & Wu, D. L. (2003). Two-day wave observations of UARS Microwave Limb Sounder mesospheric water vapor and temperature. *Journal of Geophysical Research*, *108*(D10), 4307. https://doi.org/10.1029/2002JD002903

Limpasuvan, V., & Wu, D. L. (2009). Anomalous two-day wave behavior during the 2006 austral summer. *Geophysical Research Letters*, *36*, L04807. https://doi.org/10.1092/2008GL036387

Limpasuvan, V., Wu, D. L., Schwartz, M. J., Waters, J. W., Wu, Q., & Killeen, T. L. (2005). The two-day wave in EOS MLS temperature and wind measurements during 2004-2005 winter. *Geophysical Research Letters*, *32*, L17809. https://doi.org/10.1029/2005GL023396

Lübken, F.-J., Müllemann, A., & Jarvis, M. J. (2004). Temperatures and horizontal winds in the Antarctic summer mesosphere. *Journal of Geophysical Research*, *109*, D24112. https://doi.org/10.1029/2004JD005133

Luo, Z., Fritts, D. C., Portmann, R. W., & Thomas, G. E. (1995). Dynamical and radiative forcing of the summer mesopause circulation and thermal structure, 2. Seasonal variations. *Journal of Geophysical Research*, *100*(D2), 3129–3137. https://doi.org/10.1029/94JD02517

Malinga, S. B., & Ruohoniemi, J. M. (2007). The quasi-two-day wave studied using the Northern Hemisphere superDARN HF radars. *Annales de Geophysique*, *25*(8), 1767–1778. https://doi.org/10.5194/angeo-25-1767-2007

McCormack, J., Coy, P. L., & Hoppel, K. W. (2009). Evolution of the quasi-2-day wave during January 2006. *Journal of Geophysical Research*, *114*, D20115. https://doi.org/10.1029/2009JD012239

McCormack, J. P., Eckermann, S. D., Hoppel, K. W., & Vincent, R. A. (2010). Amplification of the quasi-two day wave through nonlinear interaction with the migrating diurnal tide. *Geophysical Research Letters*, *37*, L16810. https://doi.org/10.1029/2010GL043906

McIntyre, M. E. (1989). On dynamics and transport near the polar mesopause in summer. *Journal of Geophysical Research*, *94*(D12), 14,617–14,628. https://doi.org/10.1029/JD094iD12p14617

Meek, C. E., Manson, A. H., Franke, S. J., Singer, W., Hoffmann, P., Clark, R. R., et al. (1996). Global study of Northern Hemisphere quasi-2-day wave events in recent summers near 90 km altitude. *Journal of Atmospheric and Terrestrial Physics*, *58*(13), 1401–1411. https://doi.org/10.1016/0021-9169(95)00120-4

Merzlyakov, E., Pancheva, D., Mitchell, N., Forbes, J. M., Portnyagin, Y. I., Palo, S., et al. (2004). High- and mid-latitude quasi-2-day waves observed simultaneously by four meteor radars during summer 2000. *Annales de Geophysique*, *22*(6), 1917–1929. https://doi.org/10.5194/angeo-22-1917-2004

Meyer, C. K. (1999). Gravity wave interactions with mesospheric planetary waves: A mechanism for penetration into the thermosphere-ionosphere system. *Journal of Geophysical Research*, *104*(A12), 28,181–28,196. https://doi.org/10.1029/1999JA900346

Morris, R. J., Klekouciuk, A. R., & Holdsworth, D. A. (2009). Low latitude 2-day planetary wave impact on austral polar mesopause temperatures: Revealed by a January Diminution in PMSE above Davis, Antarctica. *Geophysical Research Letters*, *36*, L11807. https://doi.org/10.1029/2009GL037817

Moudden, Y., & Forbes, J. M. (2014). Quasi-two-day wave structure, interannual variability, and tidal interactions during 2002–2011 decade. *Journal of Geophysical Research: Atmospheres*, *119*, 2241–2260. https://doi.org/10.1002/2013JD020563

Muller, H., & Kingsley, S. (1974). Long period meteor wind oscillations. *Journal of Atmospheric and Terrestrial Physics*, *36*, 1933–1943.

Muller, H., & Nelson, L. (1978). A travelling quasi-two-day wave in the meteor region. *Journal of Atmospheric and Terrestrial Physics*, *40*(6), 761–766. https://doi.org/10.1016/0021-9169(78)90136-8

Nastrom, G. D., Balsley, B. B., & Carter, D. A. (1982). Mean meridional winds in the mid- and high-latitude summer mesosphere. *Geophysical Research Letters*, *9*(2), 139–142. https://doi.org/10.1029/GL009i002p00139

Nguyen, V. A., Palo, S. E., Liebermann, R. S., Forbes, J. M., Ortland, D. A., & Siskind, D. E. (2016). Generation of secondary waves arising from nonlinear interaction between the quasi 2 day wave and the migrating diurnal tide. *Journal of Geophysical Research: Atmospheres*, *121*, 7762–7780. https://doi.org/10.1002/2016JD024794

Nguyen, V. A. (2016). Global-Scale, Nonlinearly-generated waves in the space-atmosphere interaction region. Aerospace Engineering Sciences Graduate Theses & Dissertations, 152.

Norton, W. A., & Thuburn, J. (1996). The two-day wave in a middle atmosphere GCM. *Geophysical Research Letters*, *23*(16), 2113–2116. https://doi.org/10.1029/96GL01956

Nozawa, S., Imaida, S., Brekke, A., Hall, C. M., Manson, A., Meek, C., et al. (2003). The quasi-two-day wave observed in the polar mesosphere. *Journal of Geophysical Research*, *108*(D2), 4039. https://doi.org/10.1029/2002JD002440

Offermann, D., Hoffmann, P., Knieling, P., Koppmann, R., Oberheide, J., Riggin, D. M., et al. (2011). Quasi 2 day waves in the summer mesosphere: Triple structure of amplitudes and long-term development. *Journal of Geophysical Research*, *116*, D00P02. https://doi.org/10.1029/2010JD015051

Palo, S. E., Forbes, J. M., Zhang, X., Russell, J. M., & Mlynczak, M. G. (2007). An eastward propagating two-day wave: Evidence for nonlinear planetary wave and tidal coupling in the mesosphere and lower thermosphere. *Geophysical Research Letters*, *34*, L07807. https://doi.org/10.1029/2006GL027728

Palo, S. E., Roble, R. G., & Hagan, M. E. (1999). Middle atmosphere effects of the quasi-two-day wave determined from a General Circulation Model. *Earth, Planets and Space*, *51*(7-8), 629–647. https://doi.org/10.1186/BF03353221

Pancheva, D., Mitchell, N. J., Manson, A. H., Meek, C. E., Jacobi, C., Portnyagin, Y., et al. (2004). Variability of the quasi-2-day wave observed in the MLT region during the PSMOS campaign of June-August 1999. *Journal of Atmospheric and Solar - Terrestrial Physics*, *66*(6-9), 539–565. https://doi.org/10.1016/j.jastp.2004.01.008

Pancheva, D., Mukhtarov, P., & Siskind, D. E. (2018). Climatology of the quasi-2-day waves observed in the MLS/Aura measurements (2005-2014). *Journal of Atmospheric and Solar - Terrestrial Physics*, *171*, 210–224. https://doi.org/10.1016/j.jastp.2017.05.002

Pancheva, D. V. (2006). Quasi-two-day wave and tidal variability observed over Ascension Island during January/February 2003. *Journal of Atmospheric and Terrestrial Physics*, *68*(3-5), 390–407. https://doi.org/10.1016/j.jastp.2005.02.028

Pfister, L. (1985). Baroclinic instability of easterly jets with applications to the summer mesosphere. *Journal of the Atmospheric Sciences*, *42*(4), 313–330. https://doi.org/10.1175/1520-0469(1985)042<0313:BIOEJW>2.0.CO;2

Placke, M., Hoffman, P., Becker, E., Jacobi, C., Singer, W., & Rapp, M. (2011). Gravity wave momentum fluxes in the MLT—Part II: Meteor radar investigations at high and midlatitudes in comparison with modeling studies. *Journal of Atmospheric and Solar - Terrestrial Physics*, *73*(9), 911–920. https://doi.org/10.1016/j.jastp.2010.05.007

Placke, M., Hoffmann, P., Latteck, R., & Rapp, M. (2015). Gravity wave momentum fluxes from MF and meteor radar measurements in the polar MLT region. *Journal of Geophysical Research: Space Physics*, *120*, 736–750. https://doi.org/10.1002/2014JA020460

Plumb, R. A. (1983). Baroclinic instability of the summer mesosphere: A mechanism for the quasi-two-day wave? *Journal of the Atmospheric Sciences*, *40*(1), 262–270. https://doi.org/10.1175/1520-0469(1983)040<0262:BIOTSM>2.0.CO;2

Richter, J. H., Sassi, F., & Garcia, R. R. (2010). Toward a physically based gravity wave source parameterization in a general circulation model. *Journal of the Atmospheric Sciences*, *67*(1), 136–156. https://doi.org/10.1175/2009JAS3112.1

Riggin, D. M., Lieberman, R. S., Vincent, R. A., Manson, A. H., Meek, C. E., Nakamura, T., et al. (2004). The 2-day wave during the boreal summer of 1994. *Journal of Geophysical Research*, *109*, D08110. https://doi.org/10.1029/2003JD004493

Rogers, C. D., & Prata, A. J. (1981). Evidence for a traveling two-day wave in the middle atmosphere. *Journal of Geophysical Research*, *86*(C10), 9661–9664. https://doi.org/10.1029/1C0686

Salby, M. L. (1981a). Rossby normal modes in nonuniform background configurations. I. simple fields. II—Equinox and solstice conditions. *Journal of the Atmospheric Sciences*, *38*, 1803–1840. https://doi.org/10.1175/1520-0469(1981)038<1803:RNMINB>2.0.CP;2

Salby, M. L. (1981b). Rossby normal modes in nonuniform background configurations. Part II. equinox and solstice conditions. *Journal of the Atmospheric Sciences*, *38*(9), 1827–1840. https://doi.org/10.1175/1520-0469(1981)038<1827:RNMINB>2.0.CO;2

Salby, M. L. (1981c). The 2-day wave in the middle atmosphere—Observations and theory. *Journal of Geophysical Research*, *86*(C10), 9654–9660. https://doi.org/10.1029/JC086iC10p09654

Salby, M. L., & Callagham, P. F. (2001). Seasonal amplification of the 2-day wave: Relationship between normal mode and instability. *Journal of the Atmospheric Sciences*, *58*(14), 1858–1869. https://doi.org/10.1175/1520-0469(2001)058<1858:SAOTDW>2.0.CO;2

Salby, M. L., & Callagham, P. F. (2003). Dynamics of the 2-day wave in a nonlinear model of the middle and upper atmosphere. *Journal of Geophysical Research*, *108*(D23), 4713. https://doi.org/10.1029/2003JD003648

Sandford, D. J., Schwartz, M. J., & Mitchell, N. J. (2008). The wintertime two-day wave in the polar stratosphere, mesosphere and lower thermosphere. *Atmospheric Chemistry and Physics*, *8*(3), 749–755. https://doi.org/10.5194/acp-8-749-2008

Schröder, H., & Schmitz, G. (2004). A generation mechanism for the 2-day wave near stratopause: Mixed barotropic-inertial instability. *Journal of Geophysical Research*, *109*, D24116. https://doi.org/10.1029/2004JD005177

Schwartz, M. J., Lambert, A., et al. (2008). Validation of the Aura Microwave Limb Sounder temperature and geopotential height measurements. *Journal of Geophysical Research*, *113*, D15S11. https://doi.org/10.1029/2007JD008783

Smith, A. K. (1996). Longitudinal variations in mesospheric winds: Evidence for gravity wave filtering by planetary waves. *Journal of the Atmospheric Sciences*, *53*(8), 1156–1173. https://doi.org/10.1175/1520-0469(1996)053<1156:LVIMWE>2.0.CO;2

Stockwell, R. G., Mansinha, L., & Lowe, R. P. (1996). Localization of the complex spectrum: The S transform. *IEEE Transactions on Signal Processing*, *44*(4), 998–1001. https://doi.org/10.1109/78.492555

Thayaparan, T., Hocking, W. K., MacDougall, J., Manson, A. H., & Meek, C. E. (1997). Simultaneous observations of the 2-day wave at London (43°N, 81°W) and Saskatoon (52°N, 107°W) near 91 km altitude during the two years of 1993 and 1994. *Annales de Geophysique*, *15*(10), 1324–1339. https://doi.org/10.1007/s00585-997-1324-3

Tsuda, T., Kato, S., & Vincent, R. A. (1988). Long-period wind oscillations observed by the Kyoto meteor radar and comparison of the quasi-2-day wave with Adelaide HF radar observations. *Journal of Atmospheric and Terrestrial Physics*, *50*(3), 225–230. https://doi.org/10.1016/0021-9169(88)90071-2

Tunbridge, V. M., Sandford, D. J., & Mitchell, N. J. (2011). Zonal wave numbers of the summertime 2 day planetary wave observed in the mesosphere by EOS Aura Microwave Limbe Sounder. *Journal of Geophysical Research*, *116*, D11103. https://doi.org/10.1029/2010JD014567

VanZandt, T. E., & Fritts, D. C. (1989). A theory of enhanced saturation of the gravity wave spectrum due to increases in atmospheric stability. *Pure and Applied Geophysics*, *130*(2-3), 399–420. https://doi.org/10.1007/BF00874466

Wang, D.-Y., & Fritts, D. C. (1990). Mesospheric momentum fluxes observed by the MST radar at Poker Flat, Alaska. *Journal of the Atmospheric Sciences*, *47*, 1511–1521.

Ward, W. E., Wang, D. Y., Solheim, B. H., & Shepherd, G. G. (1996). Observations of the two-day wave in WINDII data during January, 1993. *Geophysical Research Letters*, *23*(21), 2923–2926. https://doi.org/10.1029/96GL02897

Waters, J. W., Froidevaux, L., Harwood, R. S., Jarnot, R. F., Pickett, H. M., Read, W. G., et al. (2006). The Earth Observing System Microwave Limb Sounder (EOS MLS) on the Aura Satellite. *IEEE Transactions on Geoscience and Remote Sensing*, *44*(5), 1075–1092. https://doi.org/10.1109/TGRS.2006.873771

Wu, D. L., Fishben, E. F., Read, W. G., & Waters, J. W. (1996). Excitation and evolution of the quasi-2-day wave observed in UARS/MLS temperature measurements. *Journal of the Atmospheric Sciences*, *53*(5), 728–738. https://doi.org/10.1175/1520-0469(1996)053<9728:EAEOTQ>2.0.CO;2

Wu, D. L., Hays, P. B., Skinner, W. R., Marshall, A. R., Burrage, M. D., Lieberman, R. S., & Ortland, D. A. (1993). Observations of the quasi-2-day wave from the High Resolution Doppler Imager on UARS. *Geophysical Research Letters*, *20*(24), 2853–2856. https://doi.org/10.1029/93GL03008

Xian, L., Xinzchao, C., Fuller-Rowell, T., Chang, L., Fong, W., & Yu, Z. (2013). Eastward propagating planetary waves with periods of 1-5 days in the winter Antarctic stratosphere as revealed by MERRA and lidar. *Journal of Geophysical Research: Atmospheres*, *118*, 9565–9578. https://doi.org/10.1002/jgrd.50717

Yue, J., Liu, H.-L., & Chang, L. C. (2012). Numerical investigation of the quasi 2 day wave in the mesosphere and lower thermosphere. *Journal of Geophysical Research*, *117*, D05111. https://doi.org/10.1029/2011JD016574